
Exploring the Design Space of Reward Backpropagation for Flow Matching

Ruoyu Wang^{1,2,*} Boye Niu^{2,3,*} Xiangxin Zhou^{2,*} ¶‡
Yushi Huang^{2,4} Tongliang Liu³ Chi Zhang^{1,‡}

¹Westlake University ²Tencent Hunyuan

³University of Sydney ⁴The Hong Kong University of Science and Technology

*Equal contribution ¶Project Lead ‡Corresponding author

Abstract. Aligning text-to-image flow matching models with human preferences via direct reward backpropagation is sample-efficient but hampered by two well-known pathologies: activations cannot be stored across the full sampling trajectory at modern model scale, and chained Jacobian products across steps inflate the reward gradient as it travels back to early indices. Connector-based methods, such as LeapAlign, address these issues by replacing the full backward trajectory with a short pinned path, highlighting a useful decoupling between sampling and optimization. However, the quality of the resulting gradient depends on how accurately this short path approximates the full rollout, especially over long intervals. We propose FlowBP, a unified surrogate-trajectory framework that treats the backward trajectory itself as the design object. FlowBP keeps a no-gradient cached rollout for sampling, then builds a lightweight backward surrogate from cached and selectively re-forwarded velocities. This view separates four choices: the reward-model input, active set, integration weights, and bridge coupling, and recovers prior direct-gradient methods as particular settings. Within this framework, we instantiate three variants: FlowBP-Sparse uses sparse Euler reconstruction, FlowBP-Bridge adds controlled bridge coupling, and FlowBP-Lagrange raises the order of leap quadrature. All three bound memory by the active-set size and limit gradient chaining to at most one Jacobian factor. Across SD3.5-M, FLUX.1-dev, and FLUX.2-Klein-base on preference, quality, and compositional metrics, the three variants improve over direct-gradient baselines on most metrics.

Date: June 10, 2026

1 Introduction

Pretrained text-to-image flow matching models (Liu et al., 2023; Lipman et al., 2023; Esser et al., 2024; Labs, 2024; Black Forest Labs, 2026) produce high-quality images, but are not aligned with human preferences. Two post-training paradigms have emerged to close this gap. *Policy-gradient methods* (Black et al., 2024; Liu et al., 2025; Xue et al., 2025b) convert the sampler into a stochastic policy and optimize a learned reward through likelihood-style estimators. *Direct reward backpropagation* (Xu et al., 2023; Clark et al., 2024; Wu et al., 2024; Liang et al., 2026) takes a different route:

it exploits the differentiability of the flow sampler and propagates the reward gradient end-to-end through the same trajectory used at inference. The latter is sample-efficient and avoids the variance of stochastic policy gradients, but it comes with two well-known pathologies. Storing activations across the full sampling trajectory is infeasible at modern model scale, and the chained Jacobian product across steps inflates the reward gradient as it travels back (Clark et al., 2024).

At their root, the two pathologies leave any direct-gradient method facing the same four decisions: what input the reward model receives, which sampling steps carry the gradient, how their contributions are weighted, and whether a nested gradient path is retained and how it is scaled. Prior methods instantiate this surrogate in sharply different ways, but the underlying design space has not been explored. ReFL (Xu et al., 2023) keeps a single late-stage step differentiable and evaluates the reward on a one-step Tweedie estimate. DRaFT-LV (Clark et al., 2024) pins the differentiable step to the last index and reduces variance by averaging the reward gradient over multiple noise draws. DRTune (Wu et al., 2024) differentiates a sparse set of timesteps but stops the gradient at every intermediate input, deliberately removing the nested gradient path to keep the gradient bounded. LeapAlign (Liang et al., 2026) replaces the long rollout with two single-velocity hops pinned by straight-through latent connectors, retaining a nested gradient path without storing the full trajectory. This connector-based construction highlights a useful decoupling between sampling and optimization; at the same time, its gradient quality depends on how accurately the short pinned path approximates the full rollout, especially over long intervals. Each method is effective in its own regime, yet their surrogate choices were designed in isolation, leaving the underlying trade-offs and unexplored configurations unclear.

We propose FlowBP, a unified surrogate-trajectory framework that treats the backward trajectory itself as the design object. FlowBP keeps a no-gradient cached rollout for sampling, then builds a lightweight backward surrogate from cached and selectively re-forwarded velocities. Differentiating this surrogate yields a single reward gradient governed by four design axes: the *reward-model input*, the *active set*, the *integration weights*, and the *bridge coupling*. The construction bounds the original pathologies directly: memory scales with the active-set size rather than the rollout length, and gradient inflation is limited to a single Jacobian factor instead of a multi-step product. It also recovers prior methods as particular settings of the same design space: ReFL, DRaFT-LV, and DRTune use short or sparse detached surrogates whose rewards are evaluated on posterior-mean estimates, while LeapAlign uses a connector-based pinned path that keeps the reward on the sampled image and retains one nested coupling path. This map exposes several unexplored surrogate designs, motivating the three instantiations below.

We instantiate three new methods in this design space (Section 4.3). FlowBP-Sparse uses sparse Euler reconstruction: it replays cached Euler updates over the rollout, exposes only a moderate active set to autograd, drops the bridge entirely, and yields a fully decoupled gradient with no cross-step Jacobian. FlowBP-Bridge adds controlled bridge coupling by distributing a multi-step Euler active set across two segments joined by a bridge with tunable coupling strength. FlowBP-Lagrange raises the order of leap quadrature, replacing each one-velocity hop with a high-order Lagrange rule while keeping the two-segment leap structure. Evaluated on three flow-matching backbones across preference, quality, and compositional metrics, the three variants improve over the strongest direct-gradient baselines on most metrics, while their per-axis differences isolate each design choice’s contribution.

Our contributions are as follows:

- FlowBP, a unified surrogate-trajectory framework that treats the backward surrogate as the design object, subsumes prior direct-gradient methods along four axes, and bounds both memory and gradient by design.

- Three instantiations (FlowBP-Sparse, FlowBP-Bridge, and FlowBP-Lagrange) that respectively explore sparse Euler reconstruction, controlled bridge coupling, and higher-order leap quadrature.
- Consistent gains across three flow-matching backbones on preference and quality metrics, together with improved compositional generation, achieving the strongest overall results among direct-gradient methods.

2 Related Work

Preference alignment for diffusion and flow models. Recent work explores diverse post-training strategies for aligning visual generative models with human preferences. Policy-gradient and GRPO-style methods adapt RL objectives to diffusion and flow-model sampling trajectories (Black et al., 2024; Fan et al., 2023; Liu et al., 2025; Xue et al., 2025b; Li et al., 2025), while preference-optimization methods learn from paired, step-wise, dense, or self-generated preference signals (Wallace et al., 2024; Yang et al., 2024a; Liang et al., 2025; Yuan et al., 2024; Yang et al., 2024b; Zhang et al., 2026). Related likelihood- or score-based objectives further align diffusion models through score matching, discriminative optimization, or stochastic optimal control (Zhu et al., 2025; Zheng et al., 2025; Domingo-Enrich et al., 2025). Other flow or diffusion alignment methods connect online reward optimization with the model’s pretraining or forward noising process (Zheng et al., 2026; Xue et al., 2025a). These methods are broadly applicable to non-differentiable rewards, but they typically optimize stochastic trajectory objectives, preference likelihoods, control objectives, or likelihood-style surrogates rather than directly differentiating the reward through the sampler. Our work studies this complementary direct-gradient regime.

Direct reward backpropagation. Direct-gradient methods exploit the differentiability of diffusion or flow samplers to optimize reward scores without likelihood estimation (Prabhudesai et al., 2023; Xu et al., 2023; Clark et al., 2024; Wu et al., 2024; Zhang et al., 2025; Shen et al., 2025; Liang et al., 2026). Existing approaches backpropagate rewards through short late-stage denoising paths, low-variance final-step objectives, detached intermediate inputs, composition-aware feedback, full-trajectory preference signals, or learned leap trajectories. These methods demonstrate the effectiveness of differentiable rewards, but each fixes a particular choice of reward input, active denoising steps, trajectory approximation, and nested-gradient scale. Our surrogate-trajectory view makes these choices explicit and uses them as design axes for the methods studied in this paper.

3 Preliminaries

Diffusion and Flow models. Diffusion models (Ho et al., 2020; Song et al., 2021) and flow matching (Lipman et al., 2023; Liu et al., 2023) are two formulations of the same continuous-time generative process. Under the velocity parameterization (Salimans and Ho, 2022), both train a network $\mathbf{v}_\theta(\mathbf{x}_t, t, \mathbf{c})$ to predict the tangent of a trajectory $\mathbf{x}_t = \alpha_t \mathbf{x}_0 + \sigma_t \boldsymbol{\epsilon}$ that interpolates between clean data $\mathbf{x}_0 \sim p_{\text{data}}$ at $t = 0$ and Gaussian noise $\boldsymbol{\epsilon} \sim \mathcal{N}(\mathbf{0}, \mathbf{I})$ at $t = 1$. Both sample by integrating the same probability-flow ODE $d\mathbf{x}_t/dt = \mathbf{v}_\theta(\mathbf{x}_t, t, \mathbf{c})$; the two regimes differ only in the choice of noise schedule (α_t, σ_t) . Our framework treats this schedule as a hyperparameter and applies to either regime, so for concreteness we work throughout in the rectified-flow setting (Liu et al., 2023; Esser et al., 2024) ($\alpha_t = 1 - t, \sigma_t = t$).

In this setting, the straight-line interpolation $\mathbf{x}_t = (1 - t)\mathbf{x}_0 + t\boldsymbol{\epsilon}$ has target velocity $\mathbf{v} = d\mathbf{x}_t/dt = \boldsymbol{\epsilon} - \mathbf{x}_0$, and the network is trained against this target by minimizing

$$\mathcal{L}_{\text{FM}}(\theta) = \mathbb{E}_{t, \mathbf{x}_0, \boldsymbol{\epsilon}} \left[\left\| \mathbf{v}_\theta(\mathbf{x}_t, t, \mathbf{c}) - (\boldsymbol{\epsilon} - \mathbf{x}_0) \right\|_2^2 \right]. \quad (1)$$

To generate samples, we discretize reverse time into an N -step rollout with schedule $\sigma_N = 1 > \sigma_{N-1} > \dots > \sigma_0 = 0$, where $\sigma_i \in [0, 1]$ is the time (equivalently, noise level) at step i ; for example, a uniform discretization sets $\sigma_i = i/N$. Starting from initial noise $\mathbf{x}_N \sim \mathcal{N}(\mathbf{0}, \mathbf{I})$, the Euler update

$$\mathbf{x}_{i-1} = \mathbf{x}_i - (\sigma_i - \sigma_{i-1}) \mathbf{v}_i, \quad \mathbf{v}_i := \mathbf{v}_\theta(\mathbf{x}_i, \sigma_i, \mathbf{c}), \quad i = N, \dots, 1, \quad (2)$$

produces a trajectory $\{\mathbf{x}_i\}_{i=N}^0$ that terminates at the clean sample \mathbf{x}_0 . Since the rollout is fully differentiable, reward gradients can be backpropagated through any subset of these N steps to update the parameters θ (Xu et al., 2023; Clark et al., 2024; Wu et al., 2024; Liang et al., 2026).

Straight-through connectors. A common primitive used by trajectory-level reward methods such as LeapAlign (Liang et al., 2026) is the *straight-through connector*: at any rollout index i , given a differentiable surrogate estimate $\hat{\mathbf{x}}_i$, the in-place pin

$$\mathbf{x}_i = \hat{\mathbf{x}}_i + \text{sg}(\mathbf{x}_i - \hat{\mathbf{x}}_i), \quad (3)$$

keeps the forward value of \mathbf{x}_i equal to its cached value while rerouting the gradient through $\hat{\mathbf{x}}_i$, so that $\partial \mathbf{x}_i / \partial \theta = \partial \hat{\mathbf{x}}_i / \partial \theta$. Following LeapAlign, we continue to use the symbol \mathbf{x}_i for the post-connector latent. We refer to $d_i = \|\mathbf{x}_i - \hat{\mathbf{x}}_i\|_2$ as the *connector residual* at index i : it does not affect the forward value but quantifies the discrepancy between the forward and backward paths at the connection point.

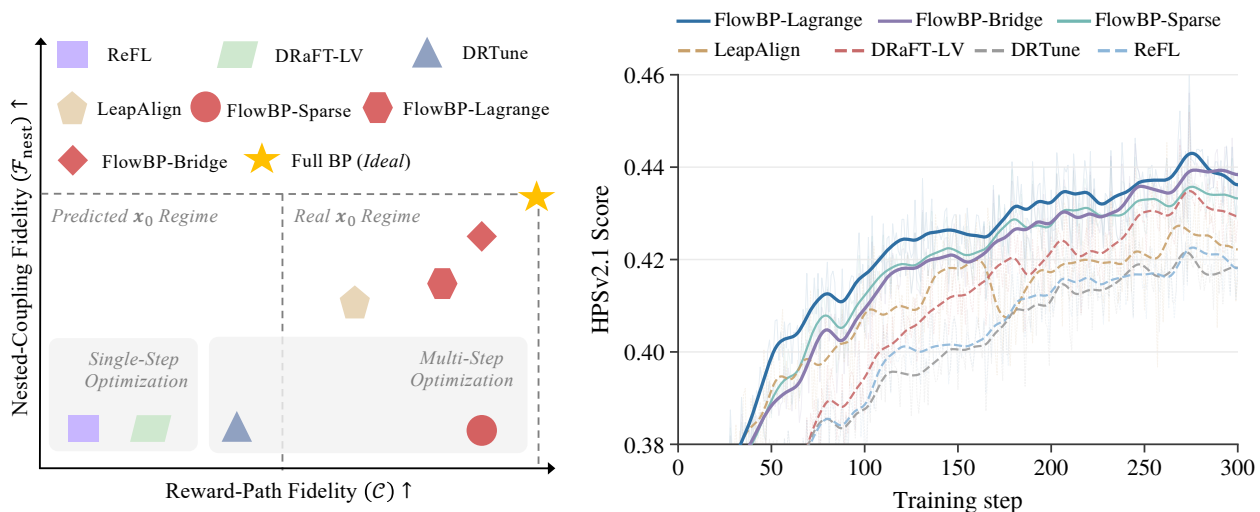


Figure 1: Overview of the FlowBP design space and empirical behavior. Left: methods are positioned by reward-path fidelity \mathcal{C} and nested-coupling fidelity $\mathcal{F}_{\text{nest}}$ (defined in Section A.1), which respectively summarize reward-input fidelity and retained cross-step gradient coupling. Right: HPSv2.1 training reward on FLUX.1-dev; our three variants optimize faster and reach higher reward than the direct-gradient baselines.

4 Method

We aim to align a pretrained flow matching model with a scalar reward $r(\mathbf{x}_0, \mathbf{c})$ by directly maximizing $\mathbb{E}[r(\mathbf{x}_0, \mathbf{c})]$ via gradient ascent. The rollout in Equation (2) is fully differentiable, so $\partial r(\mathbf{x}_0, \mathbf{c})/\partial\theta$ can in principle be obtained by reverse-mode autodiff through all N Euler steps. In practice, naive backpropagation faces two well-known obstacles, and a third arises in the connector-based remedies prior work introduces to mitigate them (Section 4.1). We address all three with a unified *surrogate-trajectory* framework (Section 4.2) that recovers ReFL (Xu et al., 2023), DRaFT-LV (Clark et al., 2024), DRTune (Wu et al., 2024), and LeapAlign (Liang et al., 2026) as special cases, motivating three new methods that improve on prior work along complementary axes: FlowBP-Sparse, FlowBP-Bridge, and FlowBP-Lagrange (Section 4.3).

4.1 Setup and Challenges

Naively computing $\partial r(\mathbf{x}_0, \mathbf{c})/\partial\theta$ by backpropagating through the Euler rollout in Equation (2) suffers from two well-documented challenges (Clark et al., 2024; Wu et al., 2024; Liang et al., 2026), and a third challenge surfaces in the connector-based remedies that prior work introduces to mitigate them.

Activation memory. Each Euler step calls \mathbf{v}_θ , whose backward pass requires the corresponding activations to be retained. Storing all N activations is prohibitive for modern backbones.

Gradient explosion. Backpropagation through the Euler chain in Equation (2) accumulates Jacobians $(\mathbf{I} - (\sigma_i - \sigma_{i-1}) \frac{\partial \mathbf{v}_\theta(\mathbf{x}_i)}{\partial \mathbf{x}_i})$ across steps, which can amplify or attenuate gradients exponentially with the number of chained steps, making gradients for early-step updates unstable (Clark et al., 2024).

Connector-induced mismatch. LeapAlign (Liang et al., 2026) constructs $\partial r(\mathbf{x}_0, \mathbf{c})/\partial\theta$ by applying the straight-through connector (3) at the rollout endpoint, but this splits the forward and backward paths there: $\nabla_{\mathbf{x}} r$ is evaluated at \mathbf{x}_0 yet composed with $\partial \hat{\mathbf{x}}_0/\partial\theta$, where $\hat{\mathbf{x}}_0$ is the connector surrogate endpoint. The mismatch scales with the connector residual $d_0 = \|\mathbf{x}_0 - \hat{\mathbf{x}}_0\|_2$, which grows when a single velocity spans a long interval; once d_0 becomes large, the surrogate gradient is no longer a reliable update direction and training destabilizes (Figure 7).

4.2 Unified Surrogate-Trajectory Framework

LeapAlign shows that straight-through connectors can avoid full-trajectory backpropagation, but its long single-velocity leaps can leave large connector residuals and route reward gradients through a biased surrogate. We address the memory, gradient-chain, and connector-mismatch issues in one surrogate-trajectory construction, reducing the mismatch either *numerically* with higher-order leap quadrature or *structurally* through Euler reconstruction that matches the rollout endpoint. We run the Euler solver in Equation (2) without autograd and cache the resulting states and velocities $\{(\mathbf{x}_i, \mathbf{v}_i)\}_{i=0}^N$; rather than backpropagating through this full rollout, we construct a lightweight surrogate trajectory on top of the cache.

The surrogate shares its forward values with the cached rollout but carries a different backward graph. Only a small subset of velocity evaluations are re-forwarded with gradients, while all other states and velocities are treated as constants. The reward is evaluated on the original rollout sample, whereas gradients flow through a sparse surrogate graph. As a result, memory scales with the number

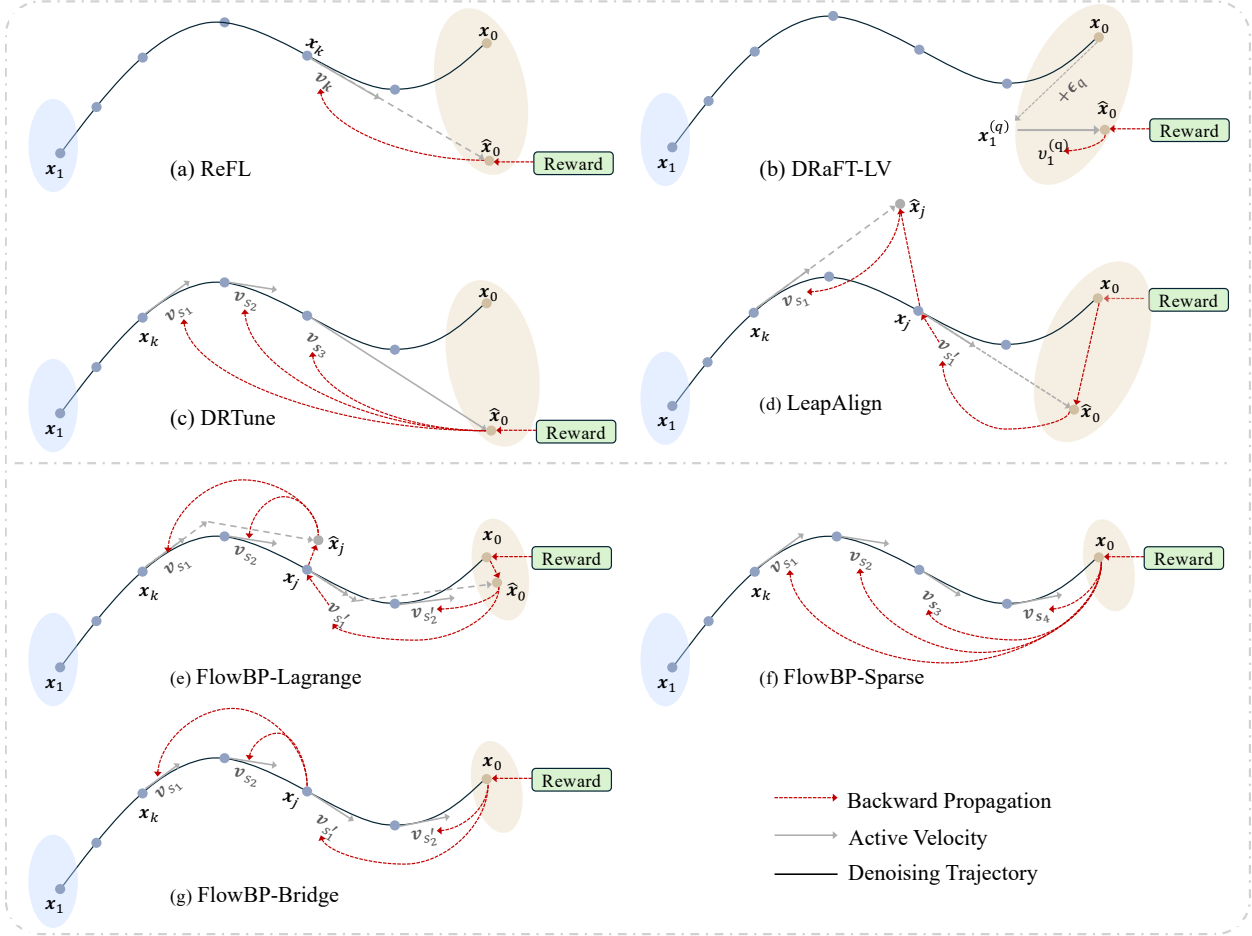


Figure 2: Surrogate backward graphs under the unified framework. Each panel uses the same cached denoising trajectory but differs in reward-model input, active velocities, integration weights, and nested-gradient path. Highlighted velocities are re-forwarded with gradients, while inactive trajectory states and velocities are detached. ReFL, DRaFT-LV, and DRiTune optimize posterior-mean endpoints with no nested path; LeapAlign keeps a two-step bridged path; FlowBP-Lagrange raises the bridge quadrature order, FlowBP-Sparse uses a sparse Euler active set without a bridge, and FlowBP-Bridge combines sparse Euler coverage with a tunable nested-gradient scale.

of active velocities rather than the rollout length N , and gradient propagation no longer traverses the full Euler chain.

For an overview of the framework and its relationship to prior methods, Figure 2 visualizes the corresponding surrogate graphs.

Surrogate structure. The surrogate approximates the cached rollout using one or two sparse segments. We use k for the noisy-side anchor of a connector-style segment and j for an optional split index, with

$$N \geq k > j \geq 0.$$

When $j = 0$, the surrogate has a single segment ending at \mathbf{x}_0 ; connector-style methods may start from \mathbf{x}_k , while Euler-reconstruction methods set $k = N$ and replay the cached rollout from \mathbf{x}_N .

When $j > 0$, the surrogate has a pre-segment and a post-segment,

$$\mathbf{x}_k \rightarrow \mathbf{x}_j \rightarrow \mathbf{x}_0,$$

with the reconstruction-based bridge using the special case $k = N$, i.e., $\mathbf{x}_N \rightarrow \mathbf{x}_j \rightarrow \mathbf{x}_0$.

Reward-model input. This axis specifies only where the scalar reward is queried. Detached short surrogates evaluate r on a posterior-mean estimate $\hat{\mathbf{x}}_0$, whereas endpoint-faithful variants make the reward read the cached rollout sample \mathbf{x}_0 . There are two ways to obtain this endpoint-faithful forward value without full-trajectory backpropagation: a straight-through endpoint connector, which keeps the forward value at \mathbf{x}_0 but differentiates through $\hat{\mathbf{x}}_0$ and is therefore sensitive to the endpoint residual $d_0 = \|\mathbf{x}_0 - \hat{\mathbf{x}}_0\|_2$; or Euler reconstruction, which replays the cached discrete updates while replacing only active velocities by re-forwarded copies, reproducing \mathbf{x}_0 by construction and eliminating endpoint connector bias.

Bridge coupling. This axis applies only when a split index j is used, and controls whether gradients from the post-segment are allowed to affect the pre-segment through the split latent. We denote the nested-gradient scale by $\alpha \in [0, 1]$. With no bridge ($j = 0$), the surrogate contains only direct active-step terms. With a bridge, the nested-gradient scale α determines how much gradient crosses the split: $\alpha = 0$ detaches the two sides, while a larger α supplies controlled cross-segment credit assignment through a single Jacobian. The bridge latent itself can be formed either by a connector, whose quality depends on the split residual $d_j = \|\mathbf{x}_j - \hat{\mathbf{x}}_j\|_2$, or by Euler reconstruction, which matches the cached \mathbf{x}_j in the forward pass and avoids a split-connector residual. Concrete realizations are given in Section 4.3.

Active set. Only a subset of velocities participates in gradient computation. We denote this active set by

$$\mathcal{A} = \mathcal{A}_{\text{pre}} \cup \mathcal{A}_{\text{post}},$$

where $\mathcal{A}_{\text{pre}} \subseteq (j, k]$ (with $k = N$ for full Euler reconstruction) and $\mathcal{A}_{\text{post}} \subseteq (0, j]$ correspond to the pre- and post-segments, respectively. We write $K = |\mathcal{A}|$ for the number of active velocities.

Each cached velocity is replaced with one of three values:

$$\tilde{\mathbf{v}}_i = \begin{cases} \mathbf{v}_\theta(\alpha \mathbf{x}_j + (1 - \alpha) \text{sg}(\mathbf{x}_j), \sigma_j, \mathbf{c}), & i = j, \\ \mathbf{v}_\theta(\text{sg}(\mathbf{x}_i), \sigma_i, \mathbf{c}), & i \in \mathcal{A}, i \neq j, \\ \text{sg}(\mathbf{v}_i), & i \notin \mathcal{A}. \end{cases} \quad (4)$$

Active steps are re-forwarded so gradients flow through θ , while their inputs remain detached to prevent gradient propagation into earlier rollout states. Inactive steps reuse the cached velocity directly. The bridge step uses the split latent \mathbf{x}_j and the coupling scale α to control whether post-segment gradients flow back into the pre-segment.

Surrogate trajectory. The cached rollout gives us the reference states $\mathbf{x}_k, \mathbf{x}_j, \mathbf{x}_0$. The surrogate graph can connect to these states in two ways. The first is a leap estimate: for an interval $s \rightarrow t$, Equation (5) predicts an approximate target and then pins it back to the cached state with the connector in Equation (3):

$$\hat{\mathbf{x}}_t = \mathbf{x}_s - \sum_{i \in [t+1, s]} w_i \tilde{\mathbf{v}}_i, \quad \mathbf{x}_t = \hat{\mathbf{x}}_t + \text{sg}(\mathbf{x}_t - \hat{\mathbf{x}}_t). \quad (5)$$

Equation (5) is lightweight, but if $\hat{\mathbf{x}}_t$ differs from the cached \mathbf{x}_t , the connector residual becomes part of the surrogate bias. The second is a reconstruction estimate: it replays the discrete Euler interval itself,

$$\mathbf{x}_t = \mathbf{x}_s - \sum_{i \in [t+1, s]} h_i \tilde{\mathbf{v}}_i, \quad h_i = \sigma_i - \sigma_{i-1}. \quad (6)$$

Because inactive velocities are the cached velocities and active velocities are re-forwarded at the same cached states, the reconstruction in Equation (6) has the same forward value as the original rollout state. Thus, reconstruction keeps the sparse backward graph but does not need a connector residual to make the reward or bridge latent lie on the cached trajectory.

Unified gradient. At the gradient level, both constructions expose the same two kinds of terms:

$$\frac{\partial \mathbf{x}_0}{\partial \theta} = \underbrace{- \sum_{i \in \mathcal{A}} w_i \frac{\partial \mathbf{v}_\theta(\mathbf{x}_i)}{\partial \theta}}_{\text{direct terms}} + \underbrace{\alpha w_j \frac{\partial \mathbf{v}_\theta(\mathbf{x}_j)}{\partial \mathbf{x}_j} \sum_{i \in \mathcal{A}_{\text{pre}}} w_i \frac{\partial \mathbf{v}_\theta(\mathbf{x}_i)}{\partial \theta}}_{\text{nested term}}. \quad (7)$$

The direct terms update each active step independently. The nested term is the only place where a Jacobian re-enters the gradient, and its depth is exactly one regardless of the rollout length N . Consequently, memory scales with $|\mathcal{A}|$ rather than N , while gradient amplification is bounded by a single Jacobian factor rather than a multi-step product.

Design axes. The unified gradient reveals four independent design choices:

- **Reward-model input:** whether the reward evaluates the rollout sample \mathbf{x}_0 or an estimate $\hat{\mathbf{x}}_0$.
- **Active set:** which velocities are re-forwarded with gradients.
- **Integration weights:** how active velocities are combined through $\{w_i\}$.
- **Bridge coupling:** whether a split index j is introduced, how the split latent is formed, and how strongly gradients couple across it through α .

As shown in Table 1, existing methods correspond to particular settings of these four axes, while our proposed variants explore previously unexplored combinations.

4.3 Method Instantiations

Table 1 maps each method onto the four axes, and prior methods cluster into two regimes. ReFL, DRaFT-LV, and DRTune never reconstruct the rollout endpoint, so the reward model reads the posterior-mean estimate $\hat{\mathbf{x}}_0$, which lies off the natural-image manifold; with no bridge, the nested term in Equation (7) vanishes, and the gradient collapses to a short direct sum with no nested gradient path. LeapAlign is the only prior method that pins both a bridge and an endpoint with connectors, but its single-velocity quadrature can incur large connector residuals over long leap intervals.

ReFL (Xu et al., 2023). A single-step active set $\mathcal{A} = \{\tau\}$ with weight $w_\tau = \sigma_\tau$ at a randomly sampled index τ corresponds to a one-step Tweedie jump $\hat{\mathbf{x}}_0 = \mathbf{x}_\tau - \sigma_\tau \mathbf{v}_\tau$ from \mathbf{x}_τ along the predicted velocity. In our framework, no endpoint or bridge connector is introduced: the reward model sees the posterior-mean estimate $\hat{\mathbf{x}}_0 = \mathbb{E}[\mathbf{x}_0 | \mathbf{x}_\tau]$, and the gradient reduces to a single direct factor $-\sigma_\tau \frac{\partial \mathbf{v}_\theta(\mathbf{x}_\tau)}{\partial \theta}$ with no nested gradient path.

Table 1: Instantiations of the unified surrogate-trajectory framework. **RM input** denotes the reward-model input, **Weights** lists the surrogate integration coefficients w_i , and **Bridge** reports the bridge setting: $j = 0$ means no bridge, while $\alpha \in (0, 1]$ sets the nested-gradient scale when a bridge is used. Here K is the cardinality of the active set ($|\mathcal{A}|$), $h_i = \sigma_i - \sigma_{i-1}$, and w_i^L denotes the Lagrange quadrature weights.

Method	RM input	Weights w_i	Active set \mathcal{A}	Bridge
ReFL (Xu et al., 2023)	$\mathbb{E}[\mathbf{x}_0 \mathbf{x}_\tau]$	$w_\tau = \sigma_\tau$	$\{\tau\}$	$j=0$
DRaFT-LV (Clark et al., 2024)	$\mathbb{E}[\mathbf{x}_0 \mathbf{x}_1]$	$w_1 = \sigma_1$	$\{1\}$	$j=0$
DRTune (Wu et al., 2024)	$\mathbb{E}[\mathbf{x}_0 \mathbf{x}_{t_{\min}}]$	Euler h_i and leap $\sigma_{t_{\min}}$	$t_{\text{train}} \cup \{t_{\min}\}$	$j=0$
LeapAlign (Liang et al., 2026)	\mathbf{x}_0	$w_k = \sigma_k - \sigma_j, w_j = \sigma_j$	$\{k, j\}, k > j$	$\alpha \in (0, 1]$
FlowBP-Sparse (ours)	\mathbf{x}_0	h_i (Euler)	K indices	$j=0$
FlowBP-Bridge (ours)	\mathbf{x}_0	h_i (Euler)	K indices, split at j	$\alpha \in (0, 1]$
FlowBP-Lagrange (ours)	\mathbf{x}_0	w_i^L (Lagrange)	$K \leq M$	$\alpha \in (0, 1]$

DRaFT-LV (Clark et al., 2024). DRaFT-LV uses the same single-step active set as ReFL but pins it to the last index ($\mathcal{A} = \{1\}$, $w_1 = \sigma_1$), with variance reduced by averaging $\nabla_x r$ over multiple noise draws at \mathbf{x}_1 . Again, no endpoint or bridge connector is introduced; the reward model sees $\hat{\mathbf{x}}_0 = \mathbb{E}[\mathbf{x}_0 | \mathbf{x}_1]$, and the nested term vanishes, leaving a single direct factor.

DRTune (Wu et al., 2024). DRTune broadens the active set to a sparse Euler quadrature over a sampled subset t_{train} of training timesteps plus a final Tweedie step at t_{\min} , with Euler weights h_i on t_{train} and weight $\sigma_{t_{\min}}$ on the Tweedie step. No endpoint or bridge connector is introduced, and the gradient is a K -summand direct sum; the reward model sees $\hat{\mathbf{x}}_0 = \mathbb{E}[\mathbf{x}_0 | \mathbf{x}_{t_{\min}}]$. DRTune therefore broadens the active set relative to ReFL and DRaFT-LV but retains their connector-free structure.

LeapAlign (Liang et al., 2026). LeapAlign is the only prior method to engage both connectors. Each segment uses a single velocity to span the full leap interval: $w_k = \sigma_k - \sigma_j$ on the pre-segment with $\mathcal{A}_{\text{pre}} = \{k\}$, and $w_j = \sigma_j$ on the post-segment with $\mathcal{A}_{\text{post}} = \{j\}$. It uses the nested-gradient scale $\alpha \in (0, 1]$ to weight the nested term. The reward sees the actual sample \mathbf{x}_0 , but $K = 2$ restricts the trajectory information the surrogate can carry. Consequently, the single-velocity bridge can produce large connector residuals d_j and d_0 over long leap intervals; when these residuals spike, the reward gradient is routed through an inaccurate bridge or endpoint estimate, making training less stable. We empirically verify the endpoint-residual failure mode in Figure 7.

Our three methods all have the reward model evaluate the actual rollout sample \mathbf{x}_0 rather than a posterior mean estimate $\hat{\mathbf{x}}_0$, but they achieve this goal in two complementary ways. We first develop reconstruction-based variants: FlowBP-Sparse reconstructs the endpoint by Euler composition while dropping the bridge, and FlowBP-Bridge additionally reconstructs the bridge with a tunable nested-gradient scale. These methods remove connector residuals structurally. We then return to the connector-based path and ask how much potential remains if we improve LeapAlign’s connector rather than replace it. This motivates FlowBP-Lagrange, which keeps the two-segment connector topology but reduces d_j and d_0 numerically by increasing both the active support and the quadrature order within each leap. We develop each method in this order below.

FlowBP-Sparse. FlowBP-Sparse uses the original Euler quadrature over the full rollout, while exposing only randomly sampled steps to autograd. In this case $j = 0$, $\mathcal{A}_{\text{pre}} = \mathcal{A}$, and $\mathcal{A}_{\text{post}} = \emptyset$, so

the composed endpoint is

$$\mathbf{x}_0 = \mathbf{x}_N - \sum_{i=1}^N h_i \tilde{\mathbf{v}}_i, \quad h_i = \sigma_i - \sigma_{i-1}, \quad (8)$$

The unified gradient in Equation (7) collapses to a clean sum,

$$\frac{\partial \mathbf{x}_0}{\partial \theta} = - \sum_{i \in \mathcal{A}} h_i \frac{\partial \mathbf{v}_\theta(\mathbf{x}_i)}{\partial \theta}, \quad (9)$$

with no nested term. Two properties follow: (i) memory is $O(K)$ regardless of N ; (ii) the gradient is bounded by K summands of bounded individual norm, eliminating gradient explosion by construction. FlowBP-Sparse thus shares the nested-free structure of ReFL, DRaFT-LV, and DRTune, but unlike them, it reconstructs the actual rollout endpoint by full Euler composition. Hence, the reward model reads the in-distribution sample \mathbf{x}_0 without bias.

FlowBP-Bridge. FlowBP-Bridge combines the full Euler-quadrature trajectory of FlowBP-Sparse with a structurally exact bridge. A split index $j \in \{1, \dots, N-1\}$ partitions the rollout into a pre-segment ($N \rightarrow j$) and a post-segment ($j \rightarrow 0$), and the K active slots are allocated approximately in proportion to segment length, with at least one active velocity on each side. Both segments use Euler weights $w_i = h_i$. The pre-segment composition reconstructs \mathbf{x}_j in the forward pass, and the velocity at the split index is re-forwarded on the discounted input from the $i = j$ branch of Equation (4) with $\alpha \in (0, 1]$. The unified gradient in Equation (7) retains both the direct sum (over both segments) and the nested term (through the bridge Jacobian $\frac{\partial \mathbf{v}_\theta(\mathbf{x}_j)}{\partial \mathbf{x}_j}$):

$$\frac{\partial \mathbf{x}_0}{\partial \theta} = - \sum_{i \in \mathcal{A}} h_i \frac{\partial \mathbf{v}_\theta(\mathbf{x}_i)}{\partial \theta} + \alpha h_j \frac{\partial \mathbf{v}_\theta(\mathbf{x}_j)}{\partial \mathbf{x}_j} \sum_{i \in \mathcal{A}_{\text{pre}}} h_i \frac{\partial \mathbf{v}_\theta(\mathbf{x}_i)}{\partial \theta}. \quad (10)$$

FlowBP-Bridge thus interpolates between FlowBP-Sparse (no bridge, fully decoupled gradient) and a one-Jacobian bridged update, trading some of FlowBP-Sparse’s decoupling guarantee for explicit nested coupling that propagates reward signals across the trajectory split. Unlike LeapAlign, this bridge is produced by Euler composition rather than by a biased single-velocity connector. Full derivations are in Section A.4.

FlowBP-Lagrange. FlowBP-Lagrange extends LeapAlign by replacing each single-velocity leap with a Lagrange quadrature rule. The two leaps span $(j, k]$ and $(0, j]$ with support sets \mathcal{S}_{pre} and $\mathcal{S}_{\text{post}}$, whose anchors are $k \in \mathcal{S}_{\text{pre}}$ and $j \in \mathcal{S}_{\text{post}}$. The gradient-active sets satisfy $\mathcal{A}_{\text{pre}} \subseteq \mathcal{S}_{\text{pre}}$ and $\mathcal{A}_{\text{post}} \subseteq \mathcal{S}_{\text{post}}$, and the active count $K = |\mathcal{A}_{\text{pre}} \cup \mathcal{A}_{\text{post}}|$ stays within a fixed active-support budget M (i.e. $K \leq M$). Integrating the segment-wise Lagrange basis polynomials gives weights w_i^L for each support; for the bridge anchor, w_j^L denotes the post-segment weight. Inactive supports, when present, are used only in the forward quadrature with detached cached velocities. The one-support-per-segment case recovers LeapAlign (Liang et al., 2026). The resulting gradient is

$$\frac{\partial \mathbf{x}_0}{\partial \theta} = - \sum_{i \in \mathcal{A}_{\text{pre}}} \rho_i w_i^L \frac{\partial \mathbf{v}_\theta(\mathbf{x}_i)}{\partial \theta} - \sum_{i \in \mathcal{A}_{\text{post}}} \rho_i w_i^L \frac{\partial \mathbf{v}_\theta(\mathbf{x}_i)}{\partial \theta} + \alpha w_j^L \frac{\partial \mathbf{v}_\theta(\mathbf{x}_j)}{\partial \mathbf{x}_j} \sum_{i \in \mathcal{A}_{\text{pre}}} \rho_i w_i^L \frac{\partial \mathbf{v}_\theta(\mathbf{x}_i)}{\partial \theta}. \quad (11)$$

Here $\rho_i = 1$ for the start anchor of each segment, while non-anchor active supports are attenuated by a fixed gradient-support scale $g_s \in [0, 1]$ (i.e. $\rho_i = g_s$) to keep the high-order correction from inflating the gradient norm. The two sums give the direct high-order support updates, and the last term is the

same single-Jacobian bridge correction as in LeapAlign, now driven by the higher-order pre-segment quadrature. Full definitions of the weights and gradient-support policy are given in Section A.2.

Design spectrum. Our three methods separate into two ways of avoiding poor reward inputs. FlowBP-Lagrange stays close to LeapAlign and reduces connector bias by raising the quadrature accuracy under a compact active-support budget, improving the per-segment integration accuracy without inflating K beyond M . FlowBP-Sparse and FlowBP-Bridge instead take a structural route to mitigating connector bias: FlowBP-Sparse increases active-step coverage while using exact Euler composition and no bridge, trading the nested gradient path for unconditional stability; FlowBP-Bridge combines a high-budget Euler active set with a structurally exact bridge and a tunable nested-gradient scale, retaining both the dense gradient signal of FlowBP-Sparse and a bounded one-step coupling path. We empirically map all three directions in Section 5.

5 Experiments

5.1 Setup

We evaluate our methods on three text-to-image flow-matching backbones spanning different model families and capacities: SD3.5-M (Esser et al., 2024), FLUX.1-dev (Labs, 2024), and FLUX.2-Klein-base (9B) (Black Forest Labs, 2026). For each backbone, we report the base model and four reward-gradient post-training baselines: ReFL (Xu et al., 2023), DRaFT-LV (Clark et al., 2024), DRTune (Wu et al., 2024), and LeapAlign (Liang et al., 2026). We implement these baselines following their official papers.

Following MixGRPO (Li et al., 2025), we evaluate all methods on the HPDv2 test split, which contains 400 held-out prompts. We use HPSv2.1 (Wu et al., 2023), PickScore (Kirstain et al., 2023), and ImageReward (Xu et al., 2023) to measure human preference alignment, and UnifiedReward-Alignment (UR-Align) and UnifiedReward-IQ (UR-IQ) (Wang et al., 2025) to assess image-text alignment and overall image quality. For each metric, we report the average score over the 400 prompts and the improvement over the corresponding base model. Since post-training uses HPSv2.1 as the differentiable reward, we treat HPSv2.1 as the in-domain metric and the remaining reward models as out-of-domain evaluators.

We further evaluate compositional generation on FLUX.1-dev using GenEval (Ghosh et al., 2023), following its official protocol, and report task accuracies and the overall score computed by the official evaluator.

5.2 Implementation Details

For our variants, we follow the LeapAlign training protocol and optimize against HPSv2.1 (Wu et al., 2023) as the differentiable reward model, using a hinge threshold of $\lambda = 0.55$. Training prompts are sampled from HPDv2. Online rollouts are generated at 512×512 resolution with 25 sampling steps. We use classifier-free guidance (Ho and Salimans, 2022) scale 3.5 for SD3.5-M and 4.0 for both FLUX backbones. We train SD3.5-M for 250 iterations and both FLUX backbones for 300 iterations. We optimize the DiT parameters with AdamW (Loshchilov and Hutter, 2019), using learning rate 1×10^{-5} , weight decay 10^{-4} , EMA decay 0.995, and batch size 64. As in LeapAlign, we use mixed-precision training with bf16 activations and maintain master weights in fp32. At

evaluation time, each checkpoint is sampled with 50 steps using the same resolution and guidance scale as training. Additional implementation details are provided in Section B.

5.3 Main Results

Table 2: Main results on three text-to-image flow-matching backbones, evaluated with HPSv2.1, PickScore, ImageReward, UR-Align, and UR-IQ. Δ denotes the improvement over the corresponding base model. Best and second-best results are shown in **bold** and underlined, respectively. Blue rows indicate our methods.

Method	In-Domain		Out-of-Domain							
	HPSv2.1		PickScore		ImageReward		UR-Align		UR-IQ	
	Score \uparrow	$\Delta(\uparrow)$	Score \uparrow	$\Delta(\uparrow)$	Score \uparrow	$\Delta(\uparrow)$	Score \uparrow	$\Delta(\uparrow)$	Score \uparrow	$\Delta(\uparrow)$
<i>SD3.5-M</i>										
SD3.5-M	0.2881	—	22.5004	—	0.9504	—	3.3935	—	3.6376	—
ReFL	0.3872	+0.0991	23.4021	+0.9017	1.3799	+0.4295	3.4779	+0.0844	3.9464	+0.3088
DRaFT-LV	0.3818	+0.0937	23.3506	+0.8502	1.3673	+0.4169	<u>3.5072</u>	<u>+0.1137</u>	3.9245	+0.2869
DR Tune	0.3870	+0.0989	23.2882	+0.7878	1.3794	+0.4290	3.4562	+0.0627	3.8869	+0.2493
LeapAlign	0.3924	+0.1043	23.3142	+0.8138	<u>1.4425</u>	<u>+0.4921</u>	3.4854	+0.0919	3.9030	+0.2654
FlowBP-Sparse	0.3939	+0.1058	23.4104	+0.9100	1.4299	+0.4795	3.4774	+0.0839	3.9690	+0.3314
FlowBP-Bridge	<u>0.3966</u>	<u>+0.1085</u>	<u>23.4130</u>	<u>+0.9126</u>	1.4386	+0.4882	3.4712	+0.0777	3.9481	+0.3105
FlowBP-Lagrange	0.3998	+0.1117	23.5040	+1.0036	1.4538	+0.5034	3.5127	+0.1192	<u>3.9680</u>	<u>+0.3304</u>
<i>FLUX.1-dev 12B</i>										
FLUX.1-dev	0.3016	—	22.5940	—	1.0094	—	3.3168	—	3.7551	—
ReFL	0.3930	+0.0914	23.6886	+1.0946	1.3916	+0.3822	3.5005	+0.1837	4.0293	+0.2742
DRaFT-LV	0.3900	+0.0884	23.6290	+1.0350	1.3910	+0.3816	3.5264	+0.2096	4.0259	+0.2708
DR Tune	0.3920	+0.0904	23.6704	+1.0764	1.4273	+0.4179	3.5403	+0.2235	4.0697	+0.3146
LeapAlign	0.4063	+0.1047	23.6158	+1.0218	1.4373	+0.4279	3.5290	+0.2122	4.0584	+0.3033
FlowBP-Sparse	0.4081	+0.1065	23.7458	+1.1518	1.4742	+0.4648	3.5408	+0.2240	4.0897	+0.3346
FlowBP-Bridge	<u>0.4119</u>	<u>+0.1103</u>	23.7952	+1.2012	1.5156	+0.5062	<u>3.5681</u>	<u>+0.2513</u>	4.1098	+0.3547
FlowBP-Lagrange	0.4134	+0.1118	<u>23.7796</u>	+1.1856	<u>1.4906</u>	<u>+0.4812</u>	3.5848	+0.2680	<u>4.0950</u>	<u>+0.3399</u>
<i>FLUX.2-Klein-base 9B</i>										
FLUX.2-Klein-base	0.2873	—	22.3158	—	1.1405	—	3.6392	—	3.7982	—
ReFL	0.4272	+0.1399	23.6002	+1.2844	1.6245	+0.4840	<u>3.6817</u>	<u>+0.0425</u>	4.0565	+0.2583
DRaFT-LV	0.4233	+0.1360	23.6288	+1.3130	1.6262	+0.4857	3.6495	+0.0103	3.9319	+0.1337
DR Tune	0.4122	+0.1249	23.5716	+1.2558	1.6264	+0.4859	3.6638	+0.0246	4.0589	+0.2607
LeapAlign	0.4246	+0.1373	23.4884	+1.1726	<u>1.6553</u>	<u>+0.5148</u>	3.6926	+0.0534	4.0625	+0.2643
FlowBP-Sparse	<u>0.4384</u>	<u>+0.1511</u>	23.8446	+1.5288	1.6649	+0.5244	3.6720	+0.0328	4.0787	+0.2805
FlowBP-Bridge	0.4387	+0.1514	<u>23.7718</u>	<u>+1.4560</u>	1.6491	+0.5086	3.6775	+0.0383	<u>4.0720</u>	<u>+0.2738</u>
FlowBP-Lagrange	0.4321	+0.1448	23.6938	+1.3780	1.6376	+0.4971	3.6705	+0.0313	4.0652	+0.2670

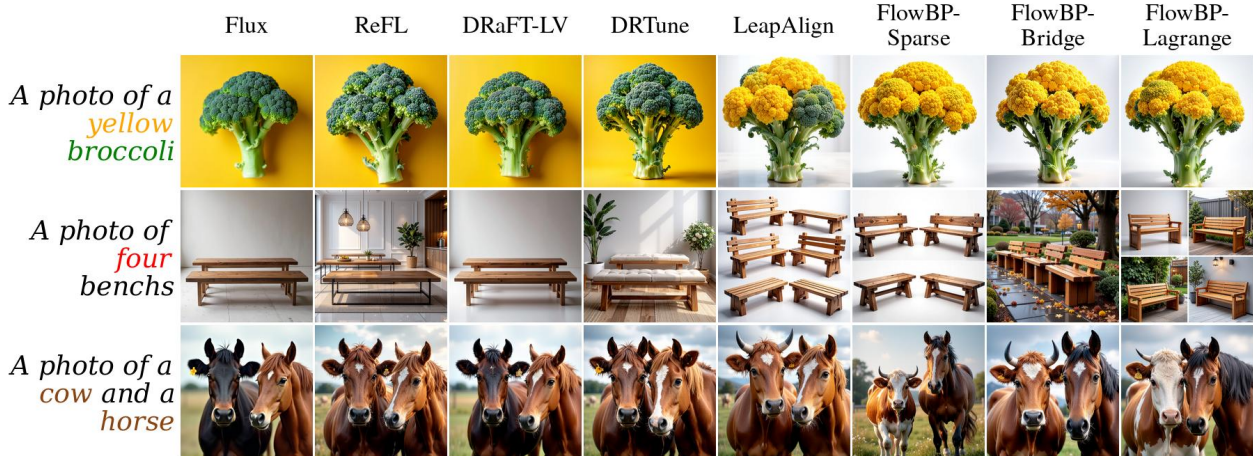


Figure 3: Qualitative comparison on GenEval prompts with FLUX.1-dev. Each row corresponds to one compositional prompt, and columns are ordered from left to right by method. The examples compare visual fidelity and prompt following under object, attribute, counting, and spatial constraints.

Table 3: GenEval results on FLUX.1-dev, including the overall score and task-level accuracies. Δ denotes the improvement over the base model. Best and second-best results are shown in **bold** and underlined, respectively. Blue rows indicate our methods.

Method	Overall		Single Obj.		Two Obj.		Count		Color		Pos		AttrB	
	Score \uparrow	$\Delta(\uparrow)$	Score \uparrow	$\Delta(\uparrow)$	Score \uparrow	$\Delta(\uparrow)$	Score \uparrow	$\Delta(\uparrow)$	Score \uparrow	$\Delta(\uparrow)$	Score \uparrow	$\Delta(\uparrow)$	Score \uparrow	$\Delta(\uparrow)$
FLUX.1-dev 12B														
FLUX.1-dev	63.25	—	97.81	—	76.52	—	70.31	—	76.86	—	17.75	—	40.25	—
ReFL	65.94	+2.69	97.50	-0.31	77.27	+0.75	71.88	+1.57	<u>78.99</u>	<u>+2.13</u>	22.25	+4.50	47.75	+7.50
DRaFT-LV	68.31	+5.06	98.13	+0.32	86.36	<u>+9.84</u>	75.00	+4.69	77.13	+0.27	23.25	+5.50	50.00	+9.75
DRTune	66.78	+3.53	<u>98.75</u>	<u>+0.94</u>	80.56	+4.04	72.81	+2.50	76.33	-0.53	20.75	+3.00	51.50	+11.25
LeapAlign	67.44	+4.19	98.44	+0.63	84.09	+7.57	72.19	+1.88	78.19	+1.33	22.25	+4.50	49.50	+9.25
FlowBP-Sparse	68.19	+4.94	<u>98.75</u>	<u>+0.94</u>	84.85	+8.33	<u>73.13</u>	<u>+2.82</u>	78.19	+1.33	22.00	+4.25	52.25	+12.00
FlowBP-Bridge	<u>68.75</u>	<u>+5.50</u>	96.88	-0.93	<u>85.10</u>	<u>+8.58</u>	70.94	+0.63	76.86	+0.00	27.25	+9.50	<u>55.50</u>	<u>+15.25</u>
FlowBP-Lagrange	69.88	+6.63	99.06	+1.25	<u>85.10</u>	<u>+8.58</u>	71.88	+1.57	79.52	+2.66	<u>23.75</u>	<u>+6.00</u>	60.00	+19.75

Table 2 reports the main comparison across the three flow-matching backbones. Across all of them, one of our variants takes the best score on nearly every preference and quality metric, with the lead rotating among the three rather than concentrating on any single variant. On SD3.5-M, FlowBP-Lagrange is strongest on HPSv2.1, PickScore, ImageReward, and UR-Align, while FlowBP-Sparse gives the best UR-IQ. On FLUX.1-dev, FlowBP-Lagrange leads on HPSv2.1 and UR-Align, whereas FlowBP-Bridge leads on PickScore, ImageReward, and UR-IQ. On FLUX.2-Klein-base, the reconstruction-based variants dominate: FlowBP-Bridge takes the best HPSv2.1 and FlowBP-Sparse the best PickScore, ImageReward, and UR-IQ. The one metric where a prior method retains the lead is UR-Align on FLUX.2-Klein-base, led by LeapAlign. Every variant improves over its base model on all five metrics, and no single variant wins everywhere; the lead shifts with backbone and reward dimension, indicating that the three variants capture genuinely different aspects of the reward landscape rather than redundant gains.

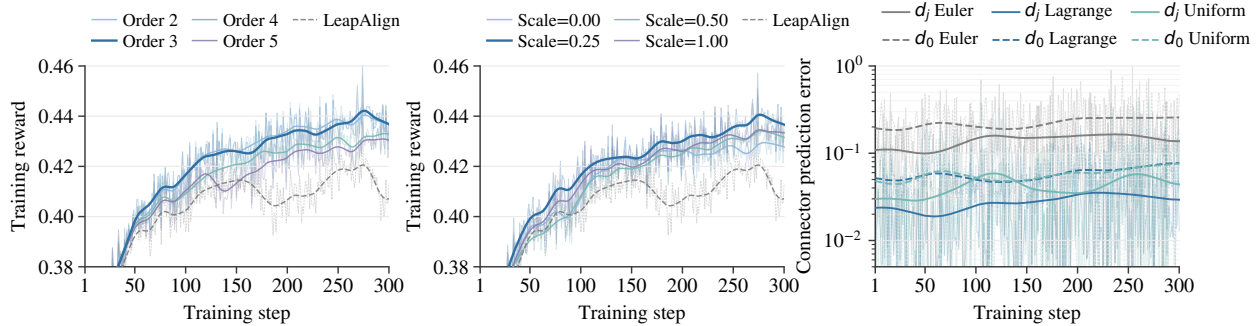


Figure 4: Ablation of FlowBP-Lagrange on **FLUX.1-dev**. Left: effect of the Lagrange quadrature order on HPSv2.1 training reward. Middle: effect of the gradient-support scale. Right: connector prediction errors for Euler, Lagrange, and uniform connectors, where uniform uses the same supports as Lagrange but replaces the integrated coefficients with equal weights.

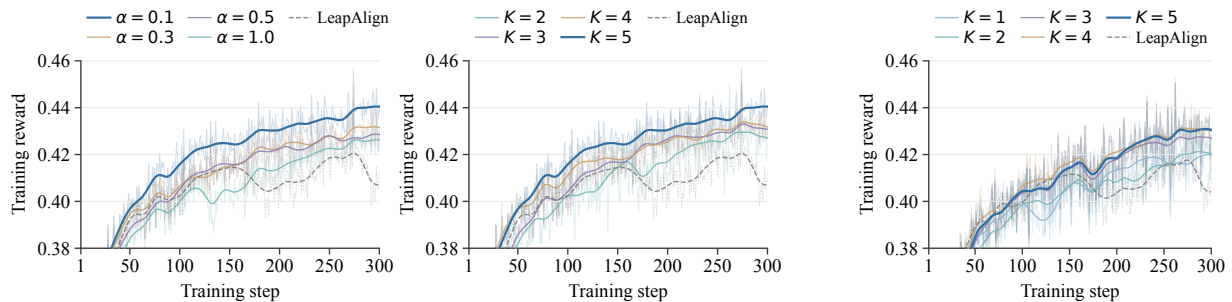


Figure 5: Ablation of FlowBP-Bridge. Left: effect of the nested-gradient scale. Right: effect of active-step budget K .

Figure 6: Ablation of FlowBP-Sparse active-step budget K .

Table 3 evaluates compositional generation on GenEval. On **FLUX.1-dev**, FlowBP-Lagrange improves the overall score from 63.25 to 69.88, achieving the best overall performance and the best scores on three categories. FlowBP-Bridge is second overall and performs best on spatial position. These results indicate that the preference improvements do not degrade compositional prompt following.

Figure 1 summarizes the design space view together with the **FLUX.1-dev** training dynamics: reward improves stably throughout optimization. Figure 3 shows representative GenEval examples consistent with the quantitative trends in Table 3. We also note that the strongest variant differs across backbones and metrics, suggesting that the surrogate-trajectory design interacts with model scale and architecture. Per-backbone evaluation dynamics over the course of training are reported in Figure 8, and additional qualitative results across all three backbones are provided in Section D.

5.4 Ablation Studies

We use **FLUX.1-dev** as the ablation backbone because it provides stable training dynamics and a representative model scale. We ablate the four design axes from Section 4.2 through the concrete knobs used by our variants: the reward-model input via endpoint reconstruction, the active set by varying the budget K , the integration weights via the different quadrature rules, and the bridge coupling via the nested-gradient scale α .

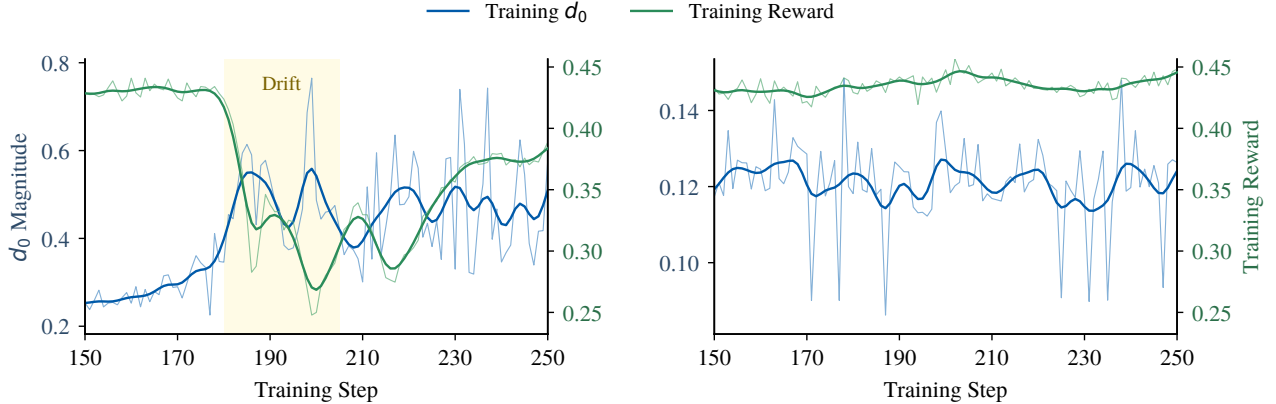


Figure 7: Connector residual and reward dynamics during training. Left: in LeapAlign, we observe that excessively large endpoint residual d_0 can coincide with reward collapse, as highlighted by the shaded interval. Right: FlowBP-Lagrange keeps d_0 smaller through the high-order connector, making this failure mode less likely during training.

Table 4: Effect of *endpoint reconstruction* on FLUX.1-dev. ReFL and DRTune evaluate the reward on the posterior-mean estimate $\hat{\mathbf{x}}_0 = \mathbb{E}[\mathbf{x}_0 | \mathbf{x}_i]$ by default. We replace this with the same Euler-reconstructed endpoint treatment used by FlowBP-Sparse (“+ endpoint recon.”), which replays the cached rollout with selected active velocities re-forwarded so the reward is evaluated on the cached sampled image \mathbf{x}_0 by construction. Δ denotes the empirical change over the same method without endpoint reconstruction. Blue rows use endpoint reconstruction.

Method	In-Domain		Out-of-Domain							
	HPSv2.1		PickScore		ImageReward		UR-Align		UR-IQ	
	Score \uparrow	$\Delta(\uparrow)$	Score \uparrow	$\Delta(\uparrow)$	Score \uparrow	$\Delta(\uparrow)$	Score \uparrow	$\Delta(\uparrow)$	Score \uparrow	$\Delta(\uparrow)$
FLUX.1-dev 12B										
ReFL	0.3930	—	23.6886	—	1.3916	—	3.5005	—	4.0293	—
+ endpoint recon.	0.3993	+0.0063	23.8121	+0.1235	1.4117	+0.0201	3.5272	+0.0267	4.0532	+0.0239
DRTune	0.3920	—	23.6704	—	1.4273	—	3.5403	—	4.0697	—
+ endpoint recon.	0.4004	+0.0085	23.7039	+0.0335	1.4576	+0.0303	3.5645	+0.0242	4.0816	+0.0119

Reward-model input. To isolate the reward-model input, we replace the posterior-mean endpoint used by ReFL and DRTune with the same Euler-composed endpoint treatment as FlowBP-Sparse: the cached rollout is replayed with the selected active velocities re-forwarded, so the forward endpoint equals the sampled image \mathbf{x}_0 by construction. This is not a straight-through endpoint connector and therefore does not introduce an endpoint pinning residual; it gives an endpoint-faithful surrogate with respect to the cached Euler rollout while keeping the active set, weights, and optimization fixed. This change improves every metric on FLUX.1-dev (Table 4), showing that placing the reward on the actual rollout sample is important even before changing the active set or quadrature rule.

FlowBP-Lagrange connector design. Figure 4 studies the two main choices in FlowBP-Lagrange: the Lagrange quadrature order and the gradient-support scale. All high-order variants use the same support points within each leap; the uniform connector simply assigns equal coefficients to these

supports, whereas the Lagrange connector computes the coefficients by integrating the Lagrange basis. The Lagrange connector attains much lower endpoint-prediction error than both the single-anchor Euler connector and the equal-weight uniform connector (right), with the gap widening over long leaps where uniform averaging still fails to track trajectory curvature. This directly explains the higher, more stable reward (left). The support scale must be balanced (middle): too small reverts to single-velocity LeapAlign, while too large overweights the high-order corrections and destabilizes training. This motivates our default, Lagrange connector with a moderate support scale; the weights and attenuation are derived in Section A.2.

FlowBP-Bridge nested-gradient scale. Figure 5 evaluates the two knobs of FlowBP-Bridge. The nested-gradient scale α interpolates from near full decoupling ($\alpha=0$, recovering FlowBP-Sparse) toward stronger nested coupling. The reward peaks at an intermediate value: moderate nested coupling propagates useful signal across the split, while strong coupling reintroduces the single-Jacobian amplification that the bridge is meant to bound. The active-step budget K controls how many denoising velocities are re-forwarded in the composed segment. The ablation shows that FlowBP-Bridge benefits from a compact but nontrivial budget, confirming that it is most useful as a controlled middle ground rather than at either extreme (gradient expression in Section A.4).

FlowBP-Sparse active-step budget. In Figure 6, we vary the active-step budget K , i.e., the number of re-forwarded velocities used in the Euler composition. Increasing K gives denser trajectory coverage but also increases the size of the backward graph. The ablation identifies a compact budget that preserves reward gains while keeping the surrogate sparse, justifying our default FlowBP-Sparse setting (Section A.3).

Connector deviation analysis. Figure 7 explains the benefit of high-order connectors. The single-velocity leap in LeapAlign incurs a large connector deviation d_0 , whose spikes coincide with reward collapse (shaded interval): once the surrogate endpoint drifts from the actual sample, the reward gradient is evaluated at an unreliable point, and training destabilizes. FlowBP-Lagrange keeps d_0 smaller via its more accurate connector, so the endpoint tracks the actual sample and training avoids this failure mode, linking its gains to a concrete, measurable mechanism.

Design takeaways. The ablations clarify how the four surrogate-design axes interact in practice. First, the reward-model input should be endpoint-faithful whenever possible: using the same endpoint reconstruction as FlowBP-Sparse already improves ReFL and DRTune across all metrics (Table 4). Second, the integration weights matter over long surrogate intervals. FlowBP-Lagrange reduces connector mismatch with a high-order quadrature rule and avoids the large d_0 failure mode observed in LeapAlign (Figure 7). Third, the active set should provide enough trajectory coverage without making the backward graph unnecessarily large; the K ablations for FlowBP-Sparse and FlowBP-Bridge both favor compact but nontrivial active budgets. Finally, bridge coupling is useful only when controlled: FlowBP-Sparse shows that detached multi-step updates are stable, while FlowBP-Bridge shows that a single α -scaled nested Jacobian can add useful cross-step credit assignment without recreating the instability of full backpropagation. Overall, a robust surrogate should place the reward on the sampled endpoint, use accurate integration over long intervals, expose a compact active set, and add bounded bridge coupling only when an additional cross-step signal is needed.

6 Conclusion

We presented FlowBP, a unified surrogate-trajectory framework for direct reward backpropagation in text-to-image flow matching models. By separating reward-model input, active-set selection,

integration weights, and bridge coupling, the framework recovers prior methods as special cases while exposing previously unexplored regions of the design space. The resulting instantiations, FlowBP-Sparse, FlowBP-Bridge, and FlowBP-Lagrange, bound memory by the number of active velocities and avoid long Jacobian chains by construction. Across three backbones and multiple preference, quality, and compositional metrics, these variants consistently improve over direct-gradient baselines, with complementary strengths across models and reward dimensions. More importantly, the results show that the four design axes provide actionable control over the surrogate backward trajectory: endpoint reconstruction improves the reward-model input, sparse active sets trade compute for trajectory coverage, higher-order integration improves long-interval accuracy, and bridge coupling adds bounded cross-step credit assignment when useful. These findings suggest that explicit surrogate-trajectory design is a practical and interpretable route for scaling reward alignment in flow-based generative models.

ACKNOWLEDGMENTS

We thank Zhanhao Liang and Yuchi Liu for insightful discussions and help.

References

- Kevin Black, Michael Janner, Yilun Du, Ilya Kostrikov, and Sergey Levine. Training diffusion models with reinforcement learning. In *The Twelfth International Conference on Learning Representations*, 2024. URL <https://openreview.net/forum?id=YCWjhGrJFD>.
- Black Forest Labs. FLUX.2 [klein]: Towards interactive visual intelligence. <https://bfl.ai/blog/flux2-klein-towards-interactive-visual-intelligence>, 2026. Model weights: <https://huggingface.co/black-forest-labs/FLUX.2-klein-base-9B>.
- Kevin Clark, Paul Vicol, Kevin Swersky, and David J. Fleet. Directly fine-tuning diffusion models on differentiable rewards. In *The Twelfth International Conference on Learning Representations*, 2024. URL <https://openreview.net/forum?id=1vmSEVL19f>.
- Carles Domingo-Enrich, Michal Drozdal, Brian Karrer, and Ricky T. Q. Chen. Adjoint matching: Fine-tuning flow and diffusion generative models with memoryless stochastic optimal control. In *The Thirteenth International Conference on Learning Representations*, 2025. URL <https://openreview.net/forum?id=xQBRrtQM8u>.
- Patrick Esser, Sumith Kulal, Andreas Blattmann, Rahim Entezari, Jonas Müller, Harry Saini, Yam Levi, Dominik Lorenz, Axel Sauer, Frederic Boesel, Dustin Podell, Tim Dockhorn, Zion English, and Robin Rombach. Scaling rectified flow transformers for high-resolution image synthesis. In *Forty-first International Conference on Machine Learning*, 2024. URL <https://openreview.net/forum?id=FPnUhsQJ5B>.
- Ying Fan, Olivia Watkins, Yuqing Du, Hao Liu, Moonkyung Ryu, Craig Boutilier, Pieter Abbeel, Mohammad Ghavamzadeh, Kangwook Lee, and Kimin Lee. Reinforcement learning for fine-tuning text-to-image diffusion models. In *Thirty-seventh Conference on Neural Information Processing Systems*, 2023. URL <https://openreview.net/forum?id=80TPepXzeh>.
- Dhruba Ghosh, Hannaneh Hajishirzi, and Ludwig Schmidt. Geneval: An object-focused framework for evaluating text-to-image alignment. In *Advances in Neural Information Processing Systems*, 2023. URL <https://openreview.net/forum?id=Wbr51vK331>.

- Jonathan Ho and Tim Salimans. Classifier-free diffusion guidance. *arXiv preprint arXiv:2207.12598*, 2022.
- Jonathan Ho, Ajay Jain, and Pieter Abbeel. Denoising diffusion probabilistic models. *Advances in neural information processing systems*, 33:6840–6851, 2020.
- Yuval Kirstain, Adam Polyak, Uriel Singer, Shahbuland Matiana, Joe Penna, and Omer Levy. Pick-a-pic: An open dataset of user preferences for text-to-image generation. In *Advances in Neural Information Processing Systems*, 2023. URL <https://arxiv.org/abs/2305.01569>.
- Black Forest Labs. FLUX. <https://github.com/black-forest-labs/flux>, 2024.
- Junzhe Li, Yutao Cui, Tao Huang, Yinping Ma, Chun Fan, Miles Yang, Zhao Zhong, and Liefeng Bo. Mixgrpo: Unlocking flow-based grpo efficiency with mixed ode-sde. *arXiv preprint arXiv:2507.21802*, 2025.
- Zhanhao Liang, Yuhui Yuan, Shuyang Gu, Bohan Chen, Tiankai Hang, Mingxi Cheng, Ji Li, and Liang Zheng. Aesthetic post-training diffusion models from generic preferences with step-by-step preference optimization. In *Proceedings of the IEEE/CVF Conference on Computer Vision and Pattern Recognition (CVPR)*, pages 13199–13208, June 2025.
- Zhanhao Liang, Tao Yang, Jie Wu, Chengjian Feng, and Liang Zheng. Leapalign: Post-training flow matching models at any generation step by building two-step trajectories. *arXiv preprint arXiv:2604.15311*, 2026.
- Yaron Lipman, Ricky T. Q. Chen, Heli Ben-Hamu, Maximilian Nickel, and Matthew Le. Flow matching for generative modeling. In *The Eleventh International Conference on Learning Representations*, 2023. URL <https://openreview.net/forum?id=PqvMRDCJT9t>.
- Jie Liu, Gongye Liu, Jiajun Liang, Yangguang Li, Jiaheng Liu, Xintao Wang, Pengfei Wan, Di Zhang, and Wanli Ouyang. Flow-grpo: Training flow matching models via online rl. *arXiv preprint arXiv:2505.05470*, 2025.
- Xingchao Liu, Chengyue Gong, and qiang liu. Flow straight and fast: Learning to generate and transfer data with rectified flow. In *The Eleventh International Conference on Learning Representations*, 2023. URL <https://openreview.net/forum?id=XVjTT1nw5z>.
- Ilya Loshchilov and Frank Hutter. Decoupled weight decay regularization. In *International Conference on Learning Representations*, 2019. URL <https://arxiv.org/abs/1711.05101>.
- Mihir Prabhudesai, Anirudh Goyal, Deepak Pathak, and Katerina Fragkiadaki. Aligning text-to-image diffusion models with reward backpropagation, 2023.
- Tim Salimans and Jonathan Ho. Progressive distillation for fast sampling of diffusion models. In *International Conference on Learning Representations*, 2022. URL <https://openreview.net/forum?id=TIIdIXIpzhoI>.
- Xiangwei Shen, Zhimin Li, Zhantao Yang, Shiyi Zhang, Yingfang Zhang, Donghao Li, Chunyu Wang, Qinglin Lu, and Yansong Tang. Directly aligning the full diffusion trajectory with fine-grained human preference, 2025. URL <https://arxiv.org/abs/2509.06942>.

- Yang Song, Jascha Sohl-Dickstein, Diederik P Kingma, Abhishek Kumar, Stefano Ermon, and Ben Poole. Score-based generative modeling through stochastic differential equations. In *International Conference on Learning Representations*, 2021. URL <https://openreview.net/forum?id=PXTIG12RRHS>.
- Bram Wallace, Meihua Dang, Rafael Rafailov, Linqi Zhou, Aaron Lou, Senthil Purushwalkam, Stefano Ermon, Caiming Xiong, Shafiq Joty, and Nikhil Naik. Diffusion model alignment using direct preference optimization. In *Proceedings of the IEEE/CVF Conference on Computer Vision and Pattern Recognition (CVPR)*, pages 8228–8238, June 2024.
- Yibin Wang, Yuhang Zang, Hao Li, Cheng Jin, and Jiaqi Wang. Unified reward model for multimodal understanding and generation. *arXiv preprint arXiv:2503.05236*, 2025.
- Xiaoshi Wu, Yiming Hao, Keqiang Sun, Yixiong Chen, Feng Zhu, Rui Zhao, and Hongsheng Li. Human preference score v2: A solid benchmark for evaluating human preferences of text-to-image synthesis. *arXiv preprint arXiv:2306.09341*, 2023.
- Xiaoshi Wu, Yiming Hao, Manyuan Zhang, Keqiang Sun, Zhaoyang Huang, Guanglu Song, Yu Liu, and Hongsheng Li. Deep reward supervisions for tuning text-to-image diffusion models. In *European Conference on Computer Vision*, pages 108–124. Springer, 2024.
- Jiazheng Xu, Xiao Liu, Yuchen Wu, Yuxuan Tong, Qinkai Li, Ming Ding, Jie Tang, and Yuxiao Dong. Imagereward: Learning and evaluating human preferences for text-to-image generation. *Advances in Neural Information Processing Systems*, 36:15903–15935, 2023.
- Shuchen Xue, Chongjian Ge, Shilong Zhang, Yichen Li, and Zhi-Ming Ma. Advantage weighted matching: Aligning rl with pretraining in diffusion models. *arXiv preprint arXiv:2509.25050*, 2025a.
- Zeyue Xue, Jie Wu, Yu Gao, Fangyuan Kong, Lingting Zhu, Mengzhao Chen, Zhiheng Liu, Wei Liu, Qiushan Guo, Weilin Huang, et al. Dancegrpo: Unleashing grpo on visual generation. *arXiv preprint arXiv:2505.07818*, 2025b.
- Kai Yang, Jian Tao, Jiafei Lyu, Chunjiang Ge, Jiabin Chen, Weihang Shen, Xiaolong Zhu, and Xiu Li. Using human feedback to fine-tune diffusion models without any reward model. In *Proceedings of the IEEE/CVF Conference on Computer Vision and Pattern Recognition*, pages 8941–8951, 2024a.
- Shentao Yang, Tianqi Chen, and Mingyuan Zhou. A dense reward view on aligning text-to-image diffusion with preference. In *Forty-first International Conference on Machine Learning*, 2024b. URL <https://openreview.net/forum?id=xVXnXk9I3I>.
- Huizhuo Yuan, Zixiang Chen, Kaixuan Ji, and Quanquan Gu. Self-play fine-tuning of diffusion models for text-to-image generation. In *The Thirty-eighth Annual Conference on Neural Information Processing Systems*, 2024. URL <https://openreview.net/forum?id=q3XavKPorV>.
- Tao Zhang, Cheng Da, Kun Ding, Huan Yang, kun jin, Yan Li, Tingting Gao, Di ZHANG, Shiming Xiang, and Chunhong Pan. Diffusion model as a noise-aware latent reward model for step-level preference optimization. In *The Thirty-ninth Annual Conference on Neural Information Processing Systems*, 2026. URL <https://openreview.net/forum?id=YB9VGCclv9>.
- Xinchen Zhang, Ling Yang, Guohao Li, YaQi Cai, xie jiake, Yong Tang, Yujiu Yang, Mengdi Wang, and Bin CUI. Itercomp: Iterative composition-aware feedback learning from model gallery for

text-to-image generation. In *The Thirteenth International Conference on Learning Representations*, 2025. URL <https://openreview.net/forum?id=4w99NAik0E>.

Kaiwen Zheng, Yongxin Chen, Huayu Chen, Guande He, Ming-Yu Liu, Jun Zhu, and Qinsheng Zhang. Direct discriminative optimization: Your likelihood-based visual generative model is secretly a GAN discriminator. In *Forty-second International Conference on Machine Learning*, 2025. URL <https://openreview.net/forum?id=0J6WE7F8tK>.

Kaiwen Zheng, Huayu Chen, Haotian Ye, Haoxiang Wang, Qinsheng Zhang, Kai Jiang, Hang Su, Stefano Ermon, Jun Zhu, and Ming-Yu Liu. DiffusionNFT: Online diffusion reinforcement with forward process. In *The Fourteenth International Conference on Learning Representations*, 2026. URL <https://openreview.net/forum?id=VJZ477R89F>.

Huasheng Zhu, Teng Xiao, and Vasant G Honavar. DSPO: Direct score preference optimization for diffusion model alignment. In *The Thirteenth International Conference on Learning Representations*, 2025. URL <https://openreview.net/forum?id=xyfb9HHvMe>.

Appendix A. Additional Derivations

This section gives the per-method derivations of the unified gradient Equation (7). We follow the notation of Section 4: the cached no-gradient rollout produces detached states and velocities $\{(\mathbf{x}_i, \mathbf{v}_i, \sigma_i)\}_{i=0}^N$ satisfying $\mathbf{x}_{i-1} = \mathbf{x}_i - h_i \mathbf{v}_i$ with $h_i = \sigma_i - \sigma_{i-1} > 0$ (cf. Equation (2)). The surrogate replaces each cached velocity with $\tilde{\mathbf{v}}_i$ from Equation (4), parameterized by an active set $\mathcal{A} = \mathcal{A}_{\text{pre}} \cup \mathcal{A}_{\text{post}}$, a bridge index j with $0 \leq j < k$, and a nested-gradient scale $\alpha \in [0, 1]$. All cached states are treated as constants during the second forward graph. Connector-based surrogates use the straight-through connector in Equation (3); reconstruction-based surrogates instead replay the cached Euler interval with $\tilde{\mathbf{v}}_i$, so their forward states equal the cached rollout states by construction.

A.1 Surrogate-Fidelity Metrics

For the diagnostic comparison in Section 4, we summarize each surrogate along two axes. Reward-path fidelity measures whether the active steps cover enough trajectory weight and whether their endpoint estimates match the actual generated sample:

$$\mathcal{C} = \frac{\sum_{i \in \mathcal{A}} w_i \left(1 - \frac{\mathbb{E}[\|\hat{\mathbf{x}}_0^{(i)} - \mathbf{x}_0\|_2]}{\mathbb{E}[\|\mathbf{x}_0\|_2]} \right)}{\sum_{i=1}^N h_i}. \quad (12)$$

Here $\hat{\mathbf{x}}_0^{(i)}$ is the endpoint estimate induced by active step i , w_i is its surrogate integration weight, h_i is the corresponding full Euler weight, and \mathcal{A} is the active set. A large \mathcal{C} therefore requires both accurate endpoint reconstruction and sufficient rollout-weight coverage. Nested-coupling fidelity instead measures whether the surrogate retains an accurate gradient path across denoising steps:

$$\mathcal{Q}_{\text{leap}} = 1 - \frac{\mathbb{E}[\|\hat{\mathbf{x}}_j - \mathbf{x}_j\|_2]}{\mathbb{E}[\|\mathbf{x}_j\|_2]}, \quad \mathcal{F}_{\text{nest}} = \frac{d_{\text{nest}}(\mathcal{M})}{N-1} \cdot \mathcal{Q}_{\text{leap}}. \quad (13)$$

Here \mathcal{M} is the surrogate backward graph, and $d_{\text{nest}}(\mathcal{M})$ counts the maximum number of inter-step Jacobian factors on any gradient path. Thus full backpropagation has $d_{\text{nest}}(\mathcal{M}) = N-1$, detached surrogates have $d_{\text{nest}}(\mathcal{M}) = 0$, and bridged surrogates have $d_{\text{nest}}(\mathcal{M}) = 1$. The argument \mathcal{M} simply makes explicit which surrogate graph is being measured. Thus \mathcal{C} describes the forward sample consumed by the reward model, whereas $\mathcal{F}_{\text{nest}}$ describes the backward coupling carried by the gradient.

A.2 FlowBP-Lagrange

FlowBP-Lagrange keeps the two-segment structure of LeapAlign but replaces each one-point leap by an integrated polynomial approximation of the velocity field. Let $k > j > 0$ be the sampled bridge indices. The quadrature supports are

$$\mathcal{S}_{\text{pre}} \subseteq \{j+1, \dots, k\}, \quad k \in \mathcal{S}_{\text{pre}}, \quad (14)$$

and analogously $\mathcal{S}_{\text{post}} \subseteq \{1, \dots, j\}$ with anchor $j \in \mathcal{S}_{\text{post}}$. The gradient-active sets satisfy $\mathcal{A}_{\text{pre}} \subseteq \mathcal{S}_{\text{pre}}$ and $\mathcal{A}_{\text{post}} \subseteq \mathcal{S}_{\text{post}}$, with $K = |\mathcal{A}_{\text{pre}} \cup \mathcal{A}_{\text{post}}| \leq M$. Inactive supports are included only in the forward quadrature through detached cached velocities, while non-anchor active supports are attenuated

during backpropagation. The pre-segment Lagrange basis polynomial associated with support $s_m \in \mathcal{S}_{\text{pre}}$ is

$$\ell_m^{\mathcal{S}_{\text{pre}}}(\sigma) = \prod_{n \neq m} \frac{\sigma - \sigma_{s_n}}{\sigma_{s_m} - \sigma_{s_n}}, \quad (15)$$

with integrated quadrature weight

$$w_{s_m}^{\text{L}} = \int_{\sigma_j}^{\sigma_k} \ell_m^{\mathcal{S}_{\text{pre}}}(\sigma) d\sigma. \quad (16)$$

Post-segment quantities $\ell_m^{\mathcal{S}_{\text{post}}}$ and $w_{s'_m}^{\text{L}}$ are constructed analogously over $[\sigma_0, \sigma_j]$. With $\sigma_j < \sigma_k$ and $\sigma_0 < \sigma_j$, the Lagrange weights are non-negative for the small per-segment support counts we use (in particular three supports per segment, which gives Simpson-like positive weights) and play the role of the positive Euler step h_i in the surrogate; we write w_i^{L} without segment subscript when the segment is clear from i (\mathcal{S}_{pre} and $\mathcal{S}_{\text{post}}$ are disjoint).

The surrogate velocity $\tilde{\mathbf{v}}_i$ at any active support $i \in \mathcal{A}$ is given by Equation (4): the post-segment anchor $i = j$ uses the bridge case $\mathbf{v}_\theta(\alpha \mathbf{x}_j + (1 - \alpha) \text{sg}(\mathbf{x}_j), \sigma_j, \mathbf{c})$, and every other active support uses the regular active case $\mathbf{v}_\theta(\text{sg}(\mathbf{x}_i), \sigma_i, \mathbf{c})$. Inactive supports use detached cached velocities in the forward quadrature. To prevent the high-order correction from inflating the gradient norm, we attenuate the contribution of non-anchor active supports through the stop-gradient identity

$$\tilde{\mathbf{v}}_i^\rho = \text{sg}(\tilde{\mathbf{v}}_i) + \rho_i(\tilde{\mathbf{v}}_i - \text{sg}(\tilde{\mathbf{v}}_i)), \quad \rho_i \in [0, 1], \quad (17)$$

with $\rho_i = 1$ for the anchor supports $i \in \{k, j\}$ and $\rho_i = g_s$ for non-anchor active supports. For inactive supports $i \notin \mathcal{A}$, we set $\tilde{\mathbf{v}}_i^\rho = \text{sg}(\mathbf{v}_i)$, so they contribute to the forward quadrature but not to the backward graph. The forward value is unchanged; the backward signal through active support i is scaled by ρ_i .

The pre-segment surrogate and bridge connector are

$$\hat{\mathbf{x}}_j = \mathbf{x}_k - \sum_{i \in \mathcal{S}_{\text{pre}}} w_i^{\text{L}} \tilde{\mathbf{v}}_i^\rho, \quad (18)$$

$$\mathbf{x}_j = \hat{\mathbf{x}}_j + \text{sg}(\mathbf{x}_j - \hat{\mathbf{x}}_j). \quad (19)$$

The just-pinned \mathbf{x}_j is the latent that enters the bridge case of Equation (4) when computing $\tilde{\mathbf{v}}_j$. The post-segment surrogate and endpoint connector are

$$\hat{\mathbf{x}}_0 = \mathbf{x}_j - \sum_{i \in \mathcal{S}_{\text{post}}} w_i^{\text{L}} \tilde{\mathbf{v}}_i^\rho, \quad (20)$$

$$\mathbf{x}_0 = \hat{\mathbf{x}}_0 + \text{sg}(\mathbf{x}_0 - \hat{\mathbf{x}}_0). \quad (21)$$

Because the bridge connector Equation (19) is transparent to gradients,

$$\frac{\partial \mathbf{x}_j}{\partial \theta} = - \sum_{i \in \mathcal{A}_{\text{pre}}} \rho_i w_i^{\text{L}} \frac{\partial \mathbf{v}_\theta(\mathbf{x}_i, \sigma_i, \mathbf{c})}{\partial \theta}. \quad (22)$$

Applying the chain rule at the bridge ($i = j$, $\rho_j = 1$) gives

$$\frac{\partial \mathbf{x}_0}{\partial \theta} = \frac{\partial \mathbf{x}_j}{\partial \theta} - \sum_{i \in \mathcal{A}_{\text{post}} \setminus \{j\}} \rho_i w_i^{\text{L}} \frac{\partial \mathbf{v}_\theta(\mathbf{x}_i, \sigma_i, \mathbf{c})}{\partial \theta} - w_j^{\text{L}} \frac{\partial \mathbf{v}_\theta(\mathbf{x}_j, \sigma_j, \mathbf{c})}{\partial \theta} - \alpha w_j^{\text{L}} \frac{\partial \mathbf{v}_\theta(\mathbf{x}_j, \sigma_j, \mathbf{c})}{\partial \mathbf{x}_j} \frac{\partial \mathbf{x}_j}{\partial \theta}. \quad (23)$$

Substituting Equation (22) and combining direct terms,

$$\frac{\partial \mathbf{x}_0}{\partial \theta} = - \sum_{i \in \mathcal{A}} \rho_i w_i^L \frac{\partial \mathbf{v}_\theta(\mathbf{x}_i, \sigma_i, \mathbf{c})}{\partial \theta} + \alpha w_j^L \frac{\partial \mathbf{v}_\theta(\mathbf{x}_j, \sigma_j, \mathbf{c})}{\partial \mathbf{x}_j} \sum_{i \in \mathcal{A}_{\text{pre}}} \rho_i w_i^L \frac{\partial \mathbf{v}_\theta(\mathbf{x}_i, \sigma_i, \mathbf{c})}{\partial \theta}. \quad (24)$$

The last term is the only nested term: it contains exactly one Jacobian factor and is scaled by α . With a single support per segment (only the segment-start anchors k and j), $w_k^L = \sigma_k - \sigma_j$ and $w_j^L = \sigma_j$, recovering the LeapAlign gradient.

A.3 FlowBP-Sparse

FlowBP-Sparse drops the bridge ($j = 0$, $\alpha = 0$, $\mathcal{A}_{\text{post}} = \emptyset$) and reconstructs the endpoint by replaying the cached trajectory with Euler weights. With no bridge, the bridge case of Equation (4) does not arise: every $i \in \mathcal{A} = \mathcal{A}_{\text{pre}}$ uses the regular active form $\mathbf{v}_\theta(\text{sg}(\mathbf{x}_i), \sigma_i, \mathbf{c})$, and every $i \notin \mathcal{A}$ uses $\text{sg}(\mathbf{v}_i)$. The endpoint reconstruction is

$$\mathbf{x}_0 = \mathbf{x}_N - \sum_{i=1}^N h_i \tilde{\mathbf{v}}_i. \quad (25)$$

Inactive velocities are detached and contribute zero to the backward pass; their forward values telescope with the active terms to match the cached \mathbf{x}_0 exactly, so no endpoint connector is needed. Since every active velocity is evaluated on a detached input, no inter-step Jacobian appears, and

$$\frac{\partial \mathbf{x}_0}{\partial \theta} = - \sum_{i \in \mathcal{A}} h_i \frac{\partial \mathbf{v}_\theta(\mathbf{x}_i, \sigma_i, \mathbf{c})}{\partial \theta}. \quad (26)$$

FlowBP-Sparse thus removes the nested gradient path in favor of a dense but fully decoupled set of direct terms.

A.4 FlowBP-Bridge

FlowBP-Bridge adds a single bridge to FlowBP-Sparse’s full Euler-quadrature trajectory. The split index $j \in \{1, \dots, N-1\}$ partitions the rollout into a pre-segment ($N \rightarrow j$) and a post-segment ($j \rightarrow 0$). The pre-segment active set $\mathcal{A}_{\text{pre}} \subseteq \{j+1, \dots, N\}$ and the post-segment active set $\mathcal{A}_{\text{post}} \subseteq \{1, \dots, j\}$ jointly form $\mathcal{A} = \mathcal{A}_{\text{pre}} \cup \mathcal{A}_{\text{post}}$, with $j \in \mathcal{A}_{\text{post}}$ as the bridge anchor. All weights are Euler weights $w_i = h_i$. Each $\tilde{\mathbf{v}}_i$ is given by Equation (4): regular active form for $i \in \mathcal{A}_{\text{pre}}$ and $i \in \mathcal{A}_{\text{post}} \setminus \{j\}$, and the bridge case at $i = j$.

The pre-segment reconstruction is

$$\mathbf{x}_j = \mathbf{x}_N - \sum_{i=j+1}^N h_i \tilde{\mathbf{v}}_i. \quad (27)$$

The post-segment endpoint reconstruction is

$$\mathbf{x}_0 = \mathbf{x}_j - \sum_{i=1}^j h_i \tilde{\mathbf{v}}_i. \quad (28)$$

Both reconstructions include inactive cached velocities, whose forward values make the reconstructed \mathbf{x}_j and \mathbf{x}_0 match the cached rollout states exactly. Since inactive velocities are detached,

$$\frac{\partial \mathbf{x}_j}{\partial \theta} = - \sum_{i \in \mathcal{A}_{\text{pre}}} h_i \frac{\partial \mathbf{v}_\theta(\mathbf{x}_i, \sigma_i, \mathbf{c})}{\partial \theta}. \quad (29)$$

At the bridge ($i = j$), the chain rule contributes both a direct term and a nested term through \mathbf{x}_j :

$$\frac{\partial \mathbf{x}_0}{\partial \theta} = \frac{\partial \mathbf{x}_j}{\partial \theta} - \sum_{i \in \mathcal{A}_{\text{post}} \setminus \{j\}} h_i \frac{\partial \mathbf{v}_\theta(\mathbf{x}_i, \sigma_i, \mathbf{c})}{\partial \theta} - h_j \frac{\partial \mathbf{v}_\theta(\mathbf{x}_j, \sigma_j, \mathbf{c})}{\partial \theta} - \alpha h_j \frac{\partial \mathbf{v}_\theta(\mathbf{x}_j, \sigma_j, \mathbf{c})}{\partial \mathbf{x}_j} \frac{\partial \mathbf{x}_j}{\partial \theta}. \quad (30)$$

Substituting Equation (29) and combining direct terms,

$$\frac{\partial \mathbf{x}_0}{\partial \theta} = - \sum_{i \in \mathcal{A}} h_i \frac{\partial \mathbf{v}_\theta(\mathbf{x}_i, \sigma_i, \mathbf{c})}{\partial \theta} + \alpha h_j \frac{\partial \mathbf{v}_\theta(\mathbf{x}_j, \sigma_j, \mathbf{c})}{\partial \mathbf{x}_j} \sum_{i \in \mathcal{A}_{\text{pre}}} h_i \frac{\partial \mathbf{v}_\theta(\mathbf{x}_i, \sigma_i, \mathbf{c})}{\partial \theta}. \quad (31)$$

This expression matches the unified gradient Equation (7): the first sum is the direct active-step update over both segments, and the last term is the bridge-induced nested term scaled by α . Setting $\alpha = 0$ removes the nested gradient path; $\alpha = 1$ preserves the full one-Jacobian bridge dependence.

Appendix B. Additional Experimental Details

Training configuration. Table 6 summarizes the common training configuration used in our experiments. All methods are trained with HPSv2.1 as the differentiable reward model and use the hinge reward loss

$$\mathcal{L}_{\text{reward}} = \text{ReLU}(\lambda - r(\mathbf{x}_0, \mathbf{c})), \quad (32)$$

where \mathbf{x}_0 is the predicted clean image, \mathbf{c} is the text prompt, and $\lambda = 0.55$. Following the LeapAlign setup, connector-based methods further apply trajectory-similarity weighting to this raw hinge loss. For a connector-based bridged surrogate, we measure the connector residuals at the bridge and clean endpoint,

$$d_j = \|\mathbf{x}_j - \hat{\mathbf{x}}_j\|_2, \quad d_0 = \|\mathbf{x}_0 - \hat{\mathbf{x}}_0\|_2, \quad (33)$$

where $\hat{\mathbf{x}}_j$ and $\hat{\mathbf{x}}_0$ are the surrogate predictions before the straight-through connectors. We then form

$$w_{\text{sim}} = \frac{1}{\max(d_j, \tau) + \max(d_0, \tau)}, \quad \mathcal{L} = \text{sg}(w_{\text{sim}}) \mathcal{L}_{\text{reward}}. \quad (34)$$

Here $\tau > 0$ is a residual floor (clamp) on d_j and d_0 , avoiding division by a near-zero denominator. The stop-gradient on w_{sim} makes d_j and d_0 act only as a scalar loss reweighting: trajectories whose surrogate connectors better match the cached rollout receive larger training weight, while the gradient-routing graph remains the one specified by the active set, integration weights, and bridge scale. For connector-based methods without an interior bridge, the same rule reduces to endpoint-deviation weighting with the d_j term omitted. Unless otherwise specified, we use loss scale 1.0, AdamW with learning rate 1×10^{-5} , weight decay 10^{-4} , no learning-rate warmup, maximum gradient norm 1.0, EMA decay 0.995, and random seed 42. Online rollouts use 25 sampling steps at 512×512 resolution. We use classifier-free guidance scale 3.5 for SD3.5-M and 4.0 for the FLUX backbones. We train SD3.5-M for 250 iterations and both FLUX.1-dev and FLUX.2-Klein-base for 300 iterations. We enable gradient checkpointing, full-shard FSDP, TF32, EMA, and bf16 mixed precision. For non-CFG-distilled models, we detach the negative branch in classifier-free guidance.

Trajectory sampling. The choice of leap indices has a direct effect on optimization stability. Uniformly sampling two indices can place the two endpoints too close to each other or too close to the noisy end of the trajectory, which increases the variance of the reward gradient. To make the training signal more stable, we use a Dirichlet sampler to partition the valid reverse-index range

Table 5: Method-specific hyperparameters used for baselines and our variants. Common optimization, reward, rollout, and precision settings are reported in Table 6. Here, K denotes the number of active steps, β is the late-bias exponent for active-step sampling, η is the gradient-rescale strength, α is the nested-gradient scale, g_s is the gradient-support scale, τ is the residual floor, and n is the number of noised samples in DRaFT-LV.

Method	Model	Hyperparameters
ReFL	All	Last-step window $N_{\text{last}} = 11$
DRaFT-LV	All	Noised samples $n = 2$
DR Tune	All	Active train steps $K = 3$; early-stop ratio 0.4
LeapAlign	All	$\alpha = 0.3$; trajectory weighting $\tau = 0.1$
FlowBP-Lagrange	Shared	Dirichlet sampler (2.5, 6.0, 2.0); $g_s = 0.25$; $\alpha = 0.1$
	SD3.5-M	$\tau = 0.2$, $k_{\text{rev}} \leq 10$, $\eta = 0$
	FLUX.1-dev	$\tau = 0.2$, $\eta = 0.5$
	FLUX.2-Klein-base	$\tau = 0.2$, $k_{\text{rev}} \leq 10$, $\eta = 0$
FlowBP-Sparse	Shared	Active steps sampled with $\Pr(i \in \mathcal{A}) \propto (N - i + 1)^\beta$
	SD3.5-M	$K = 4$, $\beta = 2$, $\eta = 0$
	FLUX.1-dev	$K = 3$, $\beta = 4$, $\eta = 1$
	FLUX.2-Klein-base	$K = 4$, $\beta = 2$, $\eta = 0$
FlowBP-Bridge	Shared	Active steps sampled with $\Pr(i \in \mathcal{A}) \propto (N - i + 1)^\beta$, $\beta = 4$
	SD3.5-M	$K = 5$, $\eta = 0.5$, $\alpha = 0.3$
	FLUX.1-dev	$K = 5$, $\eta = 1$, $\alpha = 0.1$
	FLUX.2-Klein-base	$K = 3$, $\eta = 0.5$, $\alpha = 1.0$

Table 6: Backbone-specific training configuration. All runs use HPSv2.1 as the training reward and 25-step online rollouts at 512×512 resolution.

Backbone	GPUs	Iter.	CFG	Batch	LR	WD	EMA
SD3.5-M	8×H20	250	3.5	64	1×10^{-5}	10^{-4}	0.995
FLUX.1-dev	16×H20	300	4.0	64	1×10^{-5}	10^{-4}	0.995
FLUX.2-Klein-base	16×H20	300	4.0	64	1×10^{-5}	10^{-4}	0.995

into three segments. Let $N = 25$ be the rollout length, let r_{\min} and r_{\max} denote the minimum and maximum reverse indices, and define $L = r_{\max} - r_{\min}$. We sample

$$(p_a, p_b, p_c) \sim \text{Dir}(\alpha_a, \alpha_b, \alpha_c), \quad (\alpha_a, \alpha_b, \alpha_c) = (2.5, 6.0, 2.0), \quad (35)$$

and convert the proportions into integer segment lengths

$$(\ell_a, \ell_b, \ell_c) = \text{Round}(L(p_a, p_b, p_c)), \quad \ell_a + \ell_b + \ell_c = L, \quad (36)$$

with a small correction to preserve the total length. The two reverse-time leap indices are then

$$k_{\text{rev}} = r_{\min} + \ell_a, \quad j_{\text{rev}} = r_{\min} + \ell_a + \ell_b, \quad (37)$$

and the corresponding forward-time indices are

$$k = N - k_{\text{rev}}, \quad j = N - j_{\text{rev}}, \quad 0 < j < k \leq N, \quad (38)$$

which is the strict two-segment case used by connector-style leap methods. The broader main-text convention is $N \geq k > j \geq 0$, where $j = 0$ denotes a single-segment surrogate without an interior bridge. Here, ℓ_a controls the location of k (the noisy-side endpoint for leap-style methods), ℓ_b controls the gap between k and j , and ℓ_c controls the location of j (the clean-side split). For FlowBP-Bridge, only the split j is used and the noisy-side endpoint is fixed to N , consistent with its full Euler reconstruction. Unless otherwise stated, the nested-gradient scale is 0.3.

For SD3.5-M and FLUX.2-Klein-base, we additionally cap k_{rev} at $K_{\text{max}} = 10$ to avoid unstable placements near the noisy end. When $k_{\text{rev}} > K_{\text{max}}$, we truncate the first segment and move the overflow to the last segment:

$$\ell'_a = \min(\ell_a, K_{\text{max}} - r_{\text{min}}), \quad \ell'_b = \ell_b, \quad \ell'_c = \ell_c + (\ell_a - \ell'_a). \quad (39)$$

This keeps the sampled gap ℓ_b unchanged while enforcing $k_{\text{rev}} \leq K_{\text{max}}$, which further stabilizes training.

Surrogate supports and reconstruction. All our variants first perform a no-gradient rollout to cache trajectory states and velocities, and then re-forward only selected active velocities with gradients. For FlowBP-Lagrange, an interval from s to t (with $s > t$, so $\sigma_s > \sigma_t$) is approximated by a Lagrange connector with per-leap support set \mathcal{S} ,

$$\hat{\mathbf{x}}_t = \mathbf{x}_s - \sum_{i \in \mathcal{S}} w_i \tilde{\mathbf{v}}_i, \quad w_i = \int_{\sigma_t}^{\sigma_s} \prod_{q \in \mathcal{S}, q \neq i} \frac{\sigma - \sigma_q}{\sigma_i - \sigma_q} d\sigma, \quad (40)$$

where the weights are non-negative for the small $M = |\mathcal{S}|$ we use. For FlowBP-Sparse, the clean endpoint is reconstructed with Euler weights,

$$\mathbf{x}_0 = \mathbf{x}_N - \sum_{i=1}^N h_i \tilde{\mathbf{v}}_i, \quad h_i = \sigma_i - \sigma_{i-1} > 0. \quad (41)$$

For FlowBP-Bridge, the same Euler reconstruction is applied separately on $(N \rightarrow j)$ and $(j \rightarrow 0)$. Active steps in FlowBP-Sparse and FlowBP-Bridge are sampled with a late-biased distribution $\Pr(i \in \mathcal{A}) \propto (N - i + 1)^\beta$. Since only a subset \mathcal{A} of velocities carries gradients, we use one shared gradient-rescaling rule for both high-order connectors and Euler reconstructions:

$$g = 1 + \eta \left(\frac{\sum_{i \in \mathcal{S}} |w_i|}{\sum_{i \in \mathcal{A}} |w_i|} - 1 \right), \quad (42)$$

where w_i denotes either Lagrange weights or Euler weights h_i , and $\mathcal{S} \supseteq \mathcal{A}$ is the full support or reconstruction range (the per-leap support set for FlowBP-Lagrange; $\{1, \dots, N\}$ for FlowBP-Sparse; the per-segment Euler range $\{j + 1, \dots, N\}$ or $\{1, \dots, j\}$ for FlowBP-Bridge). We apply this factor to the re-forwarded active velocity (the regular active branch of Equation (4), denoted \mathbf{v}_i below) via a stop-gradient identity,

$$\tilde{\mathbf{v}}_i = \text{sg}(\mathbf{v}_i) + g(\mathbf{v}_i - \text{sg}(\mathbf{v}_i)), \quad i \in \mathcal{A}, \quad (43)$$

So the forward trajectory is unchanged while the active velocities receive a larger effective gradient. The concrete method-specific hyperparameters are summarized in Table 5.

FLUX.2-specific implementation. For FLUX.2-Klein-base, we precompute Qwen3 text embeddings using a maximum sequence length of 512 and concatenate hidden states from layers 9, 18, and 27 as the text-conditioning representation.

Evaluation. We evaluate HPDv2 on the 400-prompt test split with 50-step sampling and report average scores and gains over the base model. GenEval results follow the official evaluator and report task accuracies and the overall score.

Evaluation dynamics. In addition to final scores, Figure 8 reports PickScore, ImageReward, and HPSv2.1 over training for all three backbones, showing whether gains persist across checkpoints.

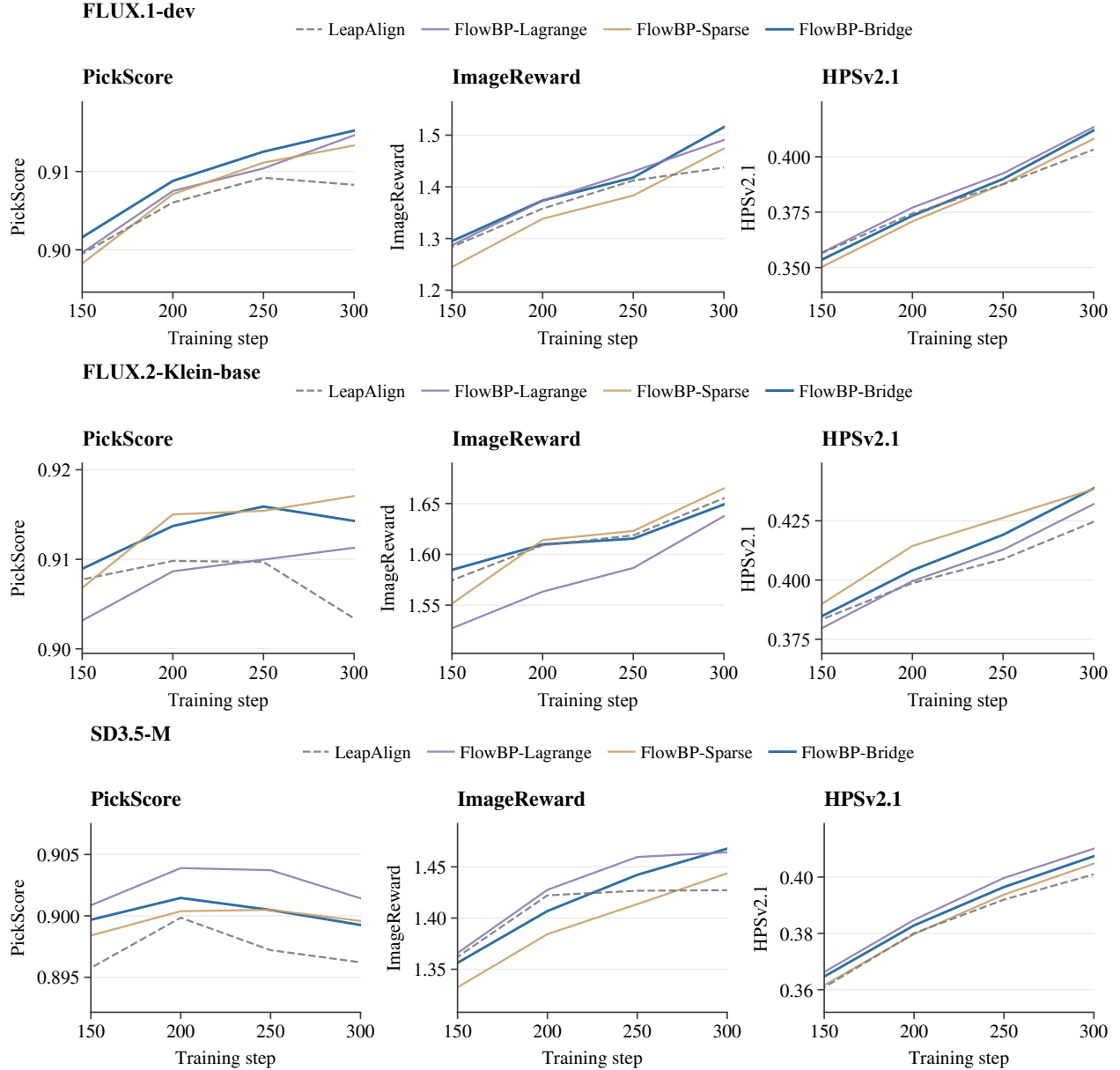


Figure 8: Evaluation dynamics on the HPDv2 test split for FLUX.1-dev, FLUX.2-Klein-base, and SD3.5-M. Each row reports PickScore, ImageReward, and HPSv2.1 over training; PickScore is normalized by 26.

Appendix C. Algorithmic Templates for Reward-Gradient Updates

This appendix specifies the reward-gradient update graphs used by the methods discussed in the main text. Each template identifies the reward input, the active velocity evaluations, and the surrogate path through which gradients are propagated.

We present two templates. Posterior-mean reward updates query the reward on a short clean estimate, whereas cached-rollout surrogate updates first sample a full trajectory without gradients and then construct a sparse backward graph on top of the cached states. Together, the two templates make the gradient-routing differences between the compared methods explicit.

C.1 Posterior-Mean Reward Updates

ReFL, DRTune, and DRaFT-LV can be written as instances of a common posterior-mean update. They differ in the stop index, the set of velocity evaluations that remain active for gradients, and the number of clean targets used to evaluate the reward. The shared template is given in Algorithm 1.

Algorithm 1: Unified Posterior-Mean Reward Updates

Input: Velocity model \mathbf{v}_θ ; reward function $r(\cdot, \cdot)$; prompt distribution p_c ; hinge threshold λ ; noise schedule $\{\sigma_i\}_{i=0}^N$; method flag $m \in \{\text{ReFL}, \text{DRTune}, \text{DRaFT-LV}\}$.

Output: Updated model parameters θ .

Unified rollout graph

- 1: Sample $\mathbf{c} \sim p_c$, $\mathbf{x}_N \sim \mathcal{N}(\mathbf{0}, \mathbf{I})$.
- 2: Choose a stop index e , active set \mathcal{A} , and clean-prediction index set \mathcal{Q} :
 - ReFL:** $(e, \mathcal{A}, \mathcal{Q}) = (\tau, \{\tau\}, \{0\})$, where $\tau \in \mathcal{T}_{\text{tail}}$.
 - DRTune:** $(e, \mathcal{A}, \mathcal{Q}) = (t_{\text{min}}, t_{\text{train}} \cup \{t_{\text{min}}\}, \{0\})$.
 - DRaFT-LV:** $(e, \mathcal{A}, \mathcal{Q}) = (1, \{1\}, \{0, \dots, n\})$.

- 3: For all executed steps, use

$$\tilde{\mathbf{v}}_i = \begin{cases} \mathbf{v}_\theta(\text{sg}(\mathbf{x}_i), \sigma_i, \mathbf{c}), & i \in \mathcal{A}, \\ \text{sg}(\mathbf{v}_\theta(\text{sg}(\mathbf{x}_i), \sigma_i, \mathbf{c})), & i \notin \mathcal{A}, \end{cases} \quad \mathbf{x}_{i-1} = \mathbf{x}_i - h_i \tilde{\mathbf{v}}_i, \quad h_i = \sigma_i - \sigma_{i-1} > 0.$$

Unified reward targets

- 4: Define the shared posterior-mean target

$$\mathbf{z}_0 = \mathbf{x}_e - \sigma_e \tilde{\mathbf{v}}_e.$$

- 5: For **DRaFT-LV** only, keep \mathbf{z}_0 as the first reward target ($q = 0$), corresponding to the direct update before re-noising. Then construct n additional low-variance targets by re-noising \mathbf{z}_0 :

$$\mathbf{x}_1^{(q)} = (1 - \sigma_1) \text{sg}(\mathbf{z}_0) + \sigma_1 \epsilon_q, \quad \mathbf{z}_q = \mathbf{x}_1^{(q)} - \sigma_1 \mathbf{v}_\theta(\text{sg}(\mathbf{x}_1^{(q)}), \sigma_1, \mathbf{c}), \quad q = 1, \dots, n.$$

Reward update

- 6: Compute $\mathcal{L} = |\mathcal{Q}|^{-1} \sum_{q \in \mathcal{Q}} \text{ReLU}(\lambda - r(\mathbf{z}_q, \mathbf{c}))$, where the single-target cases use $\mathcal{Q} = \{0\}$ and therefore only the \mathbf{z}_0 term.
 - 7: Update $\theta \leftarrow \theta - \eta \nabla_\theta \mathcal{L}$.
 - 8: **return** θ .
-

C.2 Cached-Rollout Surrogate Updates

LeapAlign and the proposed FlowBP variants use a different graph construction. They first generate and cache a complete rollout without storing activations, and then expose only selected velocity

evaluations to autograd. Connector-based variants attach sparse predictions to cached states with straight-through connectors, whereas reconstruction-based variants replay Euler updates with cached inactive velocities. Algorithm 2 summarizes this family of update graphs.

Algorithm 2: Unified Surrogate-Trajectory Gradient Methods

Input: Velocity model \mathbf{v}_θ ; scalar reward $r(\mathbf{x}_0, \mathbf{c})$; prompt distribution p_c ; hinge threshold λ ; noise schedule $\{\sigma_i\}_{i=0}^N$; method flag $m \in \{\text{LeapAlign}, \text{FlowBP-Lagrange}, \text{FlowBP-Sparse}, \text{FlowBP-Bridge}\}$.

Output: Updated model parameters θ .

Unified cached rollout

- 1: Sample $\mathbf{c} \sim p_c$, $\mathbf{x}_N \sim \mathcal{N}(\mathbf{0}, \mathbf{I})$.
- 2: Run a no-gradient rollout and cache $\{\mathbf{x}_i, \mathbf{v}_i, \sigma_i\}_{i=0}^N$.
- 3: Choose indices, active sets $\mathcal{A} = \mathcal{A}_{\text{pre}} \cup \mathcal{A}_{\text{post}}$, and weights $\{w_i\}$:
 - LeapAlign:** choose $0 < j < k \leq N$, $\mathcal{A}_{\text{pre}} = \{k\}$, $\mathcal{A}_{\text{post}} = \{j\}$, $w_k = \sigma_k - \sigma_j$, $w_j = \sigma_j$.
 - FlowBP-Lagrange:** choose $0 < j < k \leq N$, Lagrange supports \mathcal{S}_{pre} and $\mathcal{S}_{\text{post}}$ anchored at k and j , active sets $\mathcal{A}_{\text{pre}} \subseteq \mathcal{S}_{\text{pre}}$, $\mathcal{A}_{\text{post}} \subseteq \mathcal{S}_{\text{post}}$ with $|\mathcal{A}_{\text{pre}} \cup \mathcal{A}_{\text{post}}| \leq M$, and $w_i = w_i^L$.
 - FlowBP-Sparse:** $j = 0$, $\mathcal{A}_{\text{post}} = \emptyset$, $\mathcal{A} = \mathcal{A}_{\text{pre}} \subseteq \{1, \dots, N\}$, $w_i = h_i$.
 - FlowBP-Bridge:** choose $j \in \{1, \dots, N-1\}$, $\mathcal{A}_{\text{pre}} \subseteq \{j+1, \dots, N\}$, $\mathcal{A}_{\text{post}} \subseteq \{1, \dots, j\}$ with $j \in \mathcal{A}_{\text{post}}$, $w_i = h_i$.
- 4: Define active/inactive velocities (Equation (4))

Unified surrogate targets

- 5: For **FlowBP-Lagrange**, let $\tilde{\mathbf{v}}_i$ denote the Lagrange-support velocity: it follows Equation (4) when $i \in \mathcal{A}$ (including the bridge case at $i = j$), and uses the detached cached velocity $\text{sg}(\mathbf{v}_i)$ when $i \notin \mathcal{A}$.
- 6: For connector-based bridged methods, attach the pre-segment surrogate to the cached bridge state:

$$\hat{\mathbf{x}}_j = \begin{cases} \mathbf{x}_k - w_k \tilde{\mathbf{v}}_k, & \text{LeapAlign,} \\ \mathbf{x}_k - \sum_{i \in \mathcal{S}_{\text{pre}}} w_i^L \tilde{\mathbf{v}}_i, & \text{FlowBP-Lagrange,} \end{cases} \quad \mathbf{x}_j = \hat{\mathbf{x}}_j + \text{sg}(\mathbf{x}_j - \hat{\mathbf{x}}_j).$$

- 7: For **FlowBP-Bridge**, reconstruct the bridge state by Euler reconstruction

$$\mathbf{x}_j = \mathbf{x}_N - \sum_{i=j+1}^N h_i \tilde{\mathbf{v}}_i.$$

- 8: Define the clean endpoint

$$\mathbf{x}_0 = \begin{cases} \hat{\mathbf{x}}_0 + \text{sg}(\mathbf{x}_0 - \hat{\mathbf{x}}_0), & \hat{\mathbf{x}}_0 = \mathbf{x}_j - w_j \tilde{\mathbf{v}}_j, & \text{LeapAlign,} \\ \hat{\mathbf{x}}_0 + \text{sg}(\mathbf{x}_0 - \hat{\mathbf{x}}_0), & \hat{\mathbf{x}}_0 = \mathbf{x}_j - \sum_{i \in \mathcal{S}_{\text{post}}} w_i^L \tilde{\mathbf{v}}_i, & \text{FlowBP-Lagrange,} \\ \mathbf{x}_N - \sum_{i=1}^N h_i \tilde{\mathbf{v}}_i, & & \text{FlowBP-Sparse,} \\ \mathbf{x}_j - \sum_{i=1}^j h_i \tilde{\mathbf{v}}_i, & & \text{FlowBP-Bridge.} \end{cases}$$

Reward update

- 9: Compute $\mathcal{L} = \text{ReLU}(\lambda - r(\mathbf{x}_0, \mathbf{c}))$.
 - 10: Update $\theta \leftarrow \theta - \eta \nabla_\theta \mathcal{L}$ through active calls only.
 - 11: **return** θ .
-

Appendix D. Additional Qualitative Results

We provide additional qualitative examples generated from HPDv2 test prompts for SD3.5-M, FLUX.1-dev, and FLUX.2-Klein-base in Figures 9 to 11, respectively.

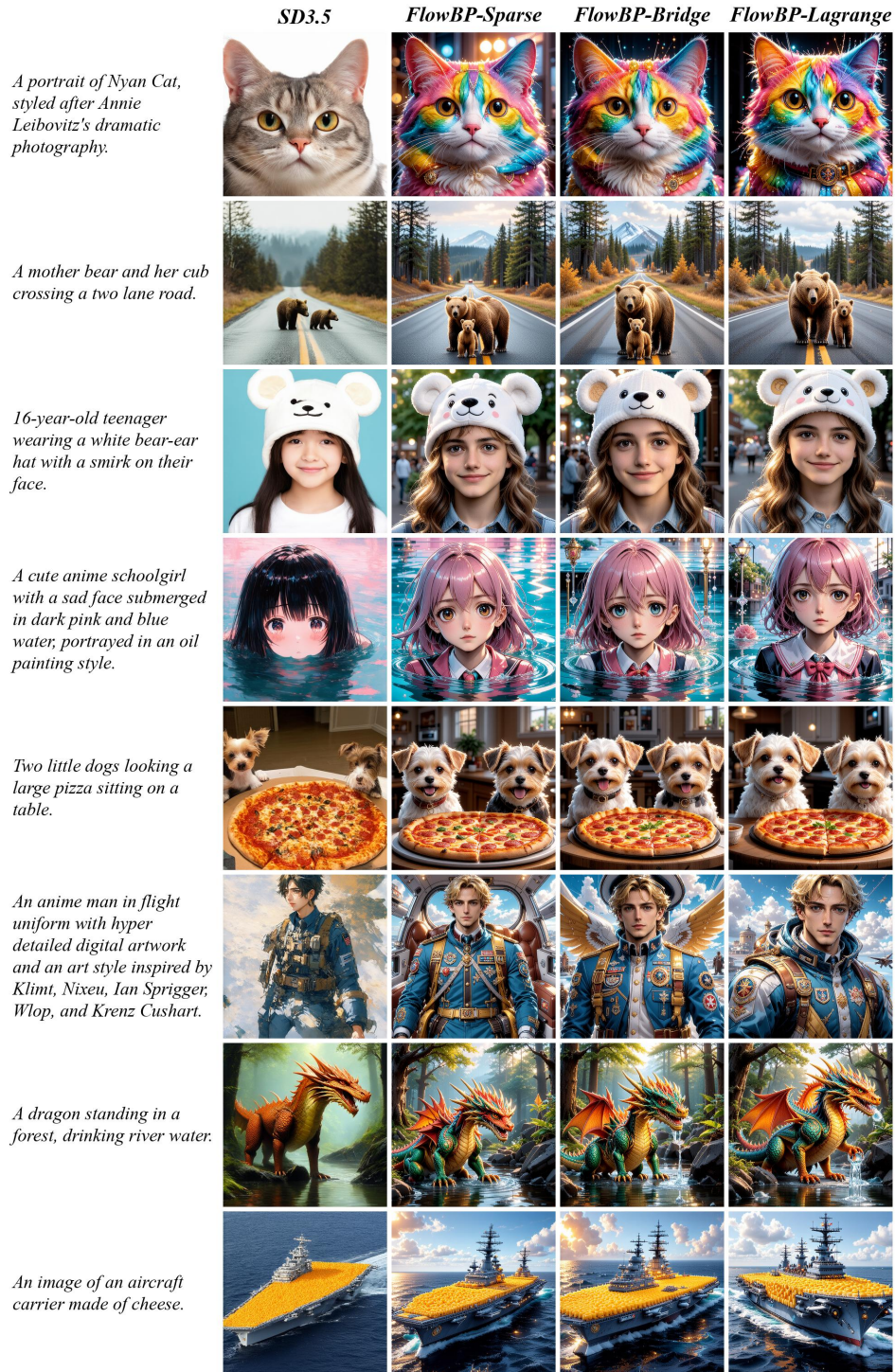


Figure 9: Additional qualitative results on SD3.5-M using prompts from the HPDv2 test split.

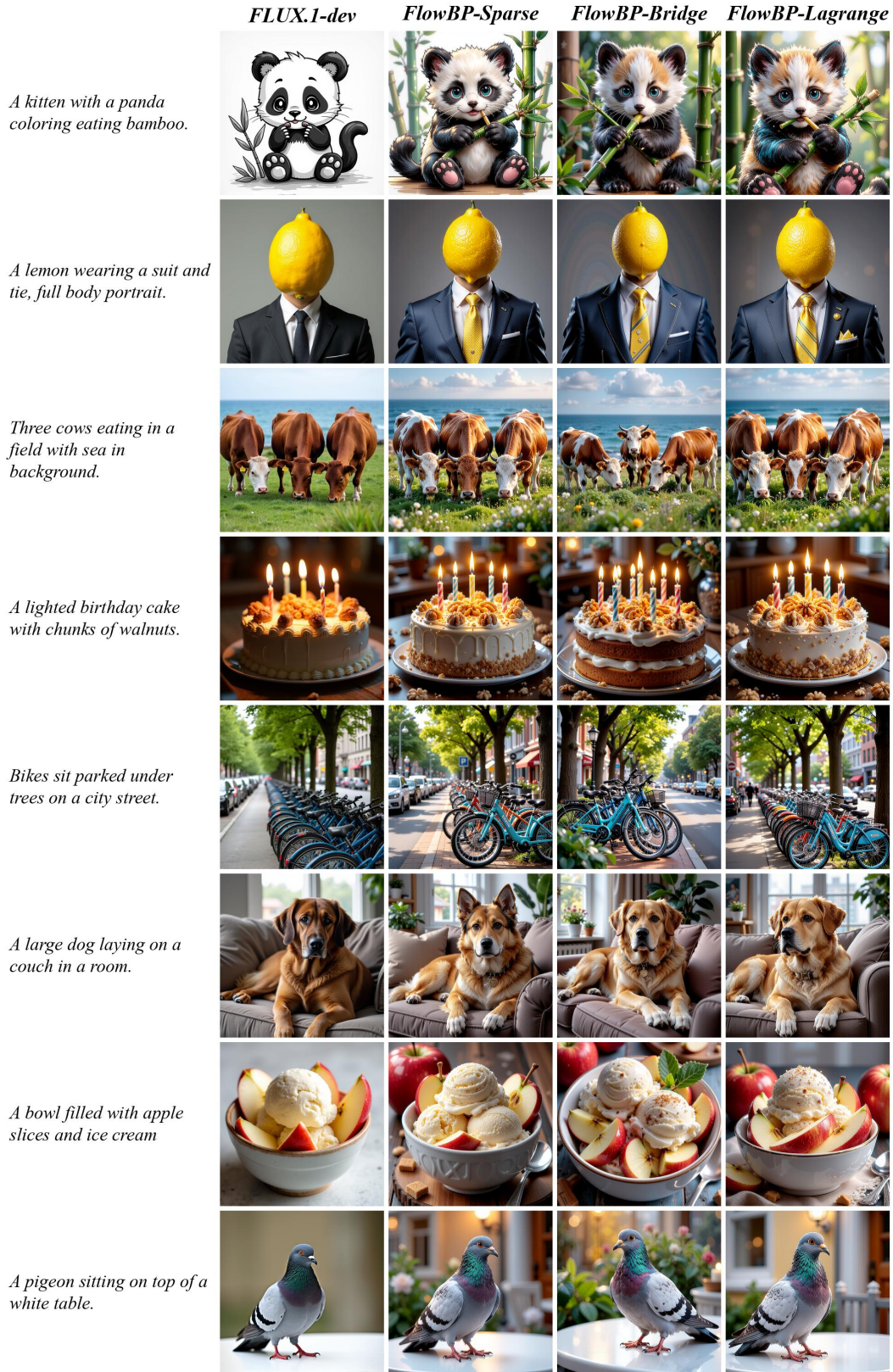


Figure 10: Additional qualitative results on FLUX.1-dev using prompts from the HPDv2 test split.



Figure 11: Additional qualitative results on FLUX.2-Klein-base using prompts from the HPDv2 test split.